MODULATED ELECTRO-HYPERTHERMIA ENHANCES THE EFFICACY OF ANTI-CANCER DRUGS IN MICE WITH TRIPLE-NEGATIVE BREAST CANCER

PhD thesis

Kenan Aloss

Semmelweis University Doctoral School, Theoretical and Translational Medicine Division

Supervisor: Péter Hamar, MD, DSc

Official reviewers: Valéria Tékus, PharmD, PhD

Tamás Szabolcs Micsik, PhD

Head of the Complex Examination Committee: Péter Sótonyi, MD, PhD

Members of the Complex Examination Committee: Tamás Radovits, MD, PhD

Hassan Charaf, DSc

Budapest

2024

Table of contents

List of abbreviations

ATG	Autophagy-related protein
BL1	Basal-like 1
BRCA	Breast cancer gene
cC3	Cleaved caspase 3
cHT	Conventional hyperthermia
DPPC	DiPalmitoyl-sn-glycero-3-PhosphoCholine
DSPC	DiStearoyl-sn-glycero-3-PhosphoCholine
DOX	Doxorubicin
ECM	Extracellular matrix
ECG	Electrocardiography
EPR	Enhanced permeability and retention
ER	Estrogen receptor (ER)
FFPE	Formalin-fixed paraffin-embedded
FOLFOX	Fluorouracil-folinic acid-oxaliplatin
H&E	Hematoxylin & Eosin
HIFU	High intensity focused ultrasound
HRP	Horse-radish peroxidase
HER-2	Human epidermal growth factor receptor
HT	Hyperthermia
IFP	Interstitial fluid pressure
IHC	Immunohistochemistry
IM	Immunomodulatory
IVIS	In vivo imaging system
LTLD	Lyso-thermosensitive liposomal doxorubicin
LAR	Luminal androgen receptor
mEHT	Modulated electro hyperthermia
MSL	Mesenchymal stem-like
MPPC	Mono-Palmitoyl-2-hydroxy-sn-glycero-3-PhosphoCholine
MSPC	Mono-Stearoyl-2-hydroxy-sn-glycero-3-PhosphoCholine
NTSL	Non-thermosensitive liposome
OS	Overall survival

PD-L1	Programmed death ligand 1
PPE	Palmar-plantar erythrodysesthesia
PEG	Polyethylene glycol
PLD	PEGylated liposomal doxorubicin
PARP	Poly (ADP-ribose) polymerase
PR	Progesterone receptor
PFS	Progression-free survival
RES	Reticuloendothelial system
RI	Resistance index
RFA	Radiofrequency ablation
SAR	Specific absorption rate
SQSTM1	Sequestosome1
TDR	Tumor destruction ratio
TNBC	Triple-negative breast cancer
TSL	Thermosensitive liposome
TTSL	Traditional thermosensitive liposome
TBF	Tumor blood flow
US	Ultrasound
WB	Western blot

1. Introduction

1.1. Triple-negative breast cancer

1.1.1. Definition, subtypes, treatment options

Triple-negative breast cancer (TNBC) is a heterogeneous breast cancer subtype that represents 10-15% of all breast cancer cases (1). TNBC is characterized by the lack of expression of estrogen receptor (ER), progesterone receptor (PR), and the human epidermal growth factor receptor (HER-2). In addition, it is common in women with breast cancer gene 1 (BRCA1) mutations (2). TNBC is highly metastatic with poor prognosis, high recurrence and mortality rates compared to other breast cancer subtypes (3). TNBC is classified into six subtypes: basal-like 1 (BL1), luminal androgen receptor (LAR), immunomodulatory (IM), mesenchymal (M), mesenchymal stem-like (MSL), and basal-like 2 (BL2) (4). The basal-like subtypes account for 70-80% of TNBC (5). The traditional protocol for TNBC treatment is based on surgery and adjuvant chemotherapy. Neoadjuvant therapy is an option for patients with inoperable TNBC. However, since TNBC cells do not express ER, PR, and HER-2, hormone and targeted therapies are ineffective. Thus, the mainstay of neoadjuvant and adjuvant treatment is conventional cytotoxic chemotherapy, such as anthracyclines and taxanes (6). Recently, immune checkpoint inhibitors, such as pembrolizumab have demonstrated survival benefits in TNBC patients (6-10). Pembrolizumab combined with chemotherapy improved the overall survival (OS) and progression-free survival (PFS) compared to placebo+chemotherapy (OS: 23 vs. 16.1 months, PFS: 9.7 vs. 5.6 months) in patients with metastatic TNBC (7, 8). However, the improvement in survival was dependent on the expression score of programmed death ligand 1 (PD-L1) (7, 8). Thus, the limited treatment options of TNBC necessitate the need for alternative treatments.

1.1.2. 4T1 mouse isograft model of triple-negative breast cancer

Various small animal models have been established in preclinical research on TNBC (11). Among these, the 4T1 mouse model stands out as widely used (12). The 4T1 cancer is an isogenic murine mammary carcinoma originally derived from a spontaneous mammary adenocarcinoma in BALB/cfC3H mice (13). 4T1 cancer has several properties that make it a suitable experimental animal model of human mammary cancer. Firstly, 4T1 cells can be easily implanted into the mouse mammary fat pad, ensuring that the primary tumor

develops in the anatomically correct location (14). Secondly, 4T1 cancers grow aggressively at the primary sites, often reaching palpable tumor size within one week after implantation (15). Thirdly, the primary tumor can later be surgically excised, which is similar to the surgical removal of the tumor in human breast cancer patients (16). Fourthly, the 4T1 cancer is highly invasive and is among a few breast cancer models that can effectively metastasize to various organs commonly affected in breast cancer, such as the lungs, liver, brain, and bone (17, 18). The metastases spontaneously develop from the primary tumor within 30 days after 4T1 cell transplantation (16). Moreover, the dissemination of 4T1 metastases to the draining lymph nodes and other organs closely resembles the pattern observed in human mammary cancer (14).

1.2. Modulated electro-hyperthermia (mEHT)

1.2.1. Principal of mEHT

Modulated electro-hyperthermia (mEHT) is an advanced option in the mild hyperthermia field, using 13.56 MHz radiofrequency electromagnetic current generated by capacitive coupling between two electrodes (Fig. 1 A) (19). mEHT is approved for cancer therapy in several countries, exhibiting promising results in different cancer types with no serious side effects (20-24). The cancer-specific effect of mEHT is based on the difference in bioelectrical properties of cancerous and healthy tissues (15). This bioelectrical difference results from the higher aerobic glycolysis of cancer cells (i.e. Warburg effect) that causes higher ion and lactate levels and thus elevates electrical conductivity of the cancer tissue (25, 26). These factors result in the selective absorption of the energy of the electromagnetic field by the cancer tissue (15). Moreover, the specific absorption rate (SAR), which refers to the rate at which electromagnetic energy is absorbed by body tissues, can be controlled, and modulated during the application of mEHT. This control allows for precise targeting of the cancer area while minimizing effects on the surrounding healthy tissues, thereby contributing to the cancer selectivity of the treatment (27).

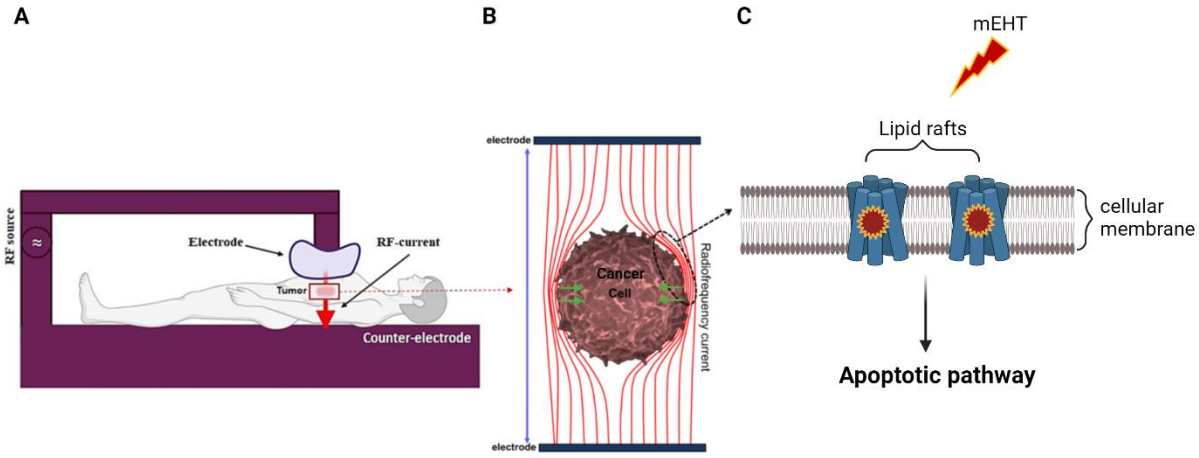

Figure 1. The principle of modulated electro-hyperthermia (mEHT). (A) In the clinic, the patient is laid on a treatment bed (i.e. the counter lower electrode), and an adjustable upper shape-adapting electrode is positioned on the body surface above the tumor. (B) The electric field (illustrated by red lines) flows from the upper electrode to the counter-electrode, enabling energy delivery to cancer cells, especially along cell membranes. (C) mEHT energy is localized mainly in lipid rafts in the cellular membrane, leading to a temperature gradient between extracellular and intracellular electrolytes, and inducing apoptotic signaling pathways (28). "Created with BioRender.com"

mEHT conveys several advantages over the conventional hyperthermia (cHT). mEHT heats the tumor selectively, archiving 2.5 °C temperature difference between the heated tumor and the surrounding tissues (15). This temperature difference does not exceed 1 ℃ in cHT (29). In contrast to cHT, the primary principle underlying mEHT was to move away from relying solely on temperature as the key factor. Instead, mEHT employs energy absorption, extracellular heating and modulation to exert its effects (29). mEHT targets the nanoscopic lipid rafts in the cellular membrane, where the major energy load is localized. Thus, mEHT delivers its energy mainly into extracellular electrolytes, establishing a temperature gradient across the cellular membrane (Fig. 1 B, C) (30). The modulation can induce non-thermal effects that improve the cell-killing thermal effects compared to cHT (31). Moreover, the measurement of SAR has resolved the main challenge encountered by all cHT devices, which is the requirement for thermometry and the complexity of intratumoral temperature measurement (28, 29). Finally, mEHT has the

advantage of being noninvasive (32) in contrast to some cHT devices (e.g. radiofrequency ablation) that require the insertion of a needle into the cancer tissue (33).

1.2.2. Effect of mEHT on the efficacy of anti-cancer drugs

mEHT can enhance the anti-cancer effects of cancer drugs by improving tumor blood flow, thus increasing drug delivery, and by exerting direct cancer cell-killing effects. Effective delivery of drugs to cancer cells relies heavily on sufficient tumor blood flow (TBF) (34). The cancer vasculature is disorganized, characterized by excessive branching. The larger, dilated vessels serve as shunts between veins and arteries, decreasing blood flow in capillaries and leading to heterogeneous distribution of blood supply in cancer tissue (35). Moreover, the increased coagulation in cancer blood vessels is another source of TBF heterogeneity (36). Therefore, the heterogeneous TBF hinders effective drug delivery to the cancer tissue (37, 38). Thus, improving TBF is the first step towards the augmentation of drug delivery to the cancer tissue.

Mild HT for 30-60 min is known to cause immediate and sustained increase in TBF (39, 40). mEHT was demonstrated to elevate TBF in cervical carcinoma patients at the end of 60 min heating (41). The main mechanism of TBF enhancement involves the vasodilation of the blood vessels in the cancer and adjacent normal tissues, as well as the reduction of blood viscosity (41). This was confirmed by a decline in the resistance index (RI) and S/D ratio (peak systolic velocity/end-diastolic velocity ratio) within blood vessels (41).

Besides improving TBF, mEHT conveys the advantage of inducing direct cellular changes in cancer cells, augmenting the efficacy of anti-cancer drugs. The direct anti-cancer effects of mEHT involves apoptosis induction (15), proliferation inhibition (19), cell cycle arrest (42), and the immunomodulatory effects (43). Thus, mEHT can synergistically improve the clinical outcome of the anti-cancer agents. In the clinic, combining mEHT with platinum-based chemotherapy in recurrent cervical cancer significantly improved the overall response (complete remission + stable disease/progressive disease) to the treatment compared to patients treated with chemotherapy alone (44). Furthermore, this combination increased the PFS compared to chemotherapy alone in cervical cancer patients with lymph node metastasis (45). In

another study, mEHT combined with 5-florouracil (5-FU), folinic acid, and oxaliplatin (FOLFOX) achieved complete pathological and clinical remission in a patient with a locally invasive rectal adenocarcinoma (46). Consistent with these findings, complete response was observed in 21 advanced ovarian cancer patients treated with a combination of mEHT, paclitaxel and carboplatin (47). Moreover, administration of mEHT in combination with bevacizumab, anti-vascular endothelial growth factor, and FOLFOX prolonged the PFS of 40 patients with metastatic colorectal cancer (48). Furthermore, the addition of mEHT to the standard treatment with chemotherapy, hormone therapy, and radiation therapy achieved partial response and disease stability in 30 % of patients with advanced breast cancer (20).

1.3. Doxorubicin

1.3.1. Mechanism of action, side effects

Doxorubicin (DOX), marketed under the brand name Adriamycin, belongs to the anthracycline class of anti-cancer drugs and stands out as one of the most potent agents within this category. It was discovered in 1969 as a byproduct of a mutated Streptomyces peucetius (49). DOX is frequently utilized, either alone or in combination with other chemotherapy medications, for the treatment of various cancer types such as breast (50), ovarian (51), bladder (52), and lung (53). Its mechanism of action involves intercalating into the DNA and subsequently inhibiting topoisomerase-II-mediated DNA repair (54). Additionally, the cytotoxicity of DOX is attributed to the significant role played by the generation of free radicals (55). Ultimately, DOX results in cancer cell death (56). DOX-induced apoptosis is mainly a caspase-dependent apoptosis, which is characterized by the elevation of cleaved caspase-3 (cC3), the main effector of apoptosis (57). Furthermore, DOX inhibits cancer cell proliferation, demonstrated by reduced Ki67 expression, a commonly used proliferation marker (58).

Despite its efficacy, the utilization of DOX is constrained by the occurrence of adverse effects, notably cardiotoxicity (59) and myelosuppression (60). The primary dose-limiting side effect of DOX is cumulative dose-related cardiotoxicity (59). In the clinic, the cumulative DOX dose is typically capped at 400–450 mg/m^2 (61). Nevertheless, even

at lower cumulative doses (approximately 300 mg/m2), subclinical cardiomyopathy may still manifest (62).

The severity of DOX-induced cardiotoxicity can range from asymptomatic electrocardiography (ECG) changes to decompensated cardiomyopathy characterized by a reduced left ventricular ejection fraction. DOX-induced cardiotoxicity can be categorized into three types: acute, early-onset chronic, and late-onset chronic (63). Acute toxicity is relatively uncommon, occurring either during or shortly after the completion of the treatment. It manifests as pericarditis, tachycardia, and ECG changes, including T-wave flattening in the left chest lead (v3–6) and prolonged QT intervals (64). The early-onset chronic toxicity appears within a year following DOX administration, while the late-onset chronic toxicity occurs one or more years after treatment cessation (65). Chronic toxicity is primarily characterized by congestive heart failure, with a 36% risk of incidence at cumulative doses exceeding 600 mg/m2 (66).

1.3.2. Limitations of the FDA-approved liposomal doxorubicin formulations

Several strategies have been exploited to enhance the efficacy and safety profile of DOX. The most common approach is encapsulation into liposomes. Two liposomal formulations of DOX have been approved for clinical application: PEGylated liposomal DOX (PLD), marketed as Doxil® or Lipodox® (generic Doxil®) in the US and Caelyx® in Europe, and non-PEGylated liposomal DOX known as Myocet®, available in Europe and Canada (67). The authorized formulations have demonstrated a decrease in cardiotoxicity and haematological toxicity compared to free DOX (68, 69). PEGylation, which involves attaching polyethylene glycol (PEG), has been utilized to extend circulation half-life and decrease uptake by the reticuloendothelial system (RES) (70). PLD extravasates through the porous vasculature of tumors, leading to improved delivery to the cancer site (71). The primary toxicity associated with PLD is the mucosal and cutaneous toxicity, which limits the administered dose (72). Hand-foot syndrome, also referred to as palmar-plantar erythrodysesthesia (PPE), is the term used to describe the mucocutaneous toxicity (73). Although the mechanism of this dose-limiting adverse effect is not fully elucidated, it is partially attributed to the presence of the PEG group

and the long circulation half-life. Furthermore, the local pressure was demonstrated to contribute to the PLD-associated PPE (73, 74). The role of local pressure was confirmed after observing PPE syndrome in other skin areas subject to frequent contact pressure or microtrauma such as groins and axillae (74). In contrast, patients treated with non-PEGylated liposomal DOX (Myocet) did not experience PPE syndrome, underscoring the involvement of PEG in this toxicity (75).

Although the authorized formulations offer improved safety profiles, their therapeutic effectiveness, as determined by PFS and OS, is not superior to conventional DOX (68, 69). This non-superiority has been attributed to several potential mechanisms:

- Inadequate release of DOX from the liposome (76).
- Entrapment of the liposome within cellular lysosomes, restricting its delivery to the nucleus and reducing its bioavailability (77).
- Tumor delivery of liposomes rely solely on the enhanced permeability and retention (EPR) effect of the tumor (Fig. 2). Thus, they can passively extravasate through the leaky vasculature of the tumor into the tumor interstitium. However, this extravasation can be limited by:
    - The significant heterogeneity of the EPR effect within the tumor and between cancer types (78)
    - Certain cancer types, like pancreatic cancer, demonstrate poor EPR due to dense fibrous tissue (79), while hematologic malignancies such as leukaemia and lymphoma do not exhibit the EPR effect (80).
    - Most solid cancers are characterized by elevated interstitial fluid pressure (IFP) (81), which further complicates the distribution of liposomes. Interaction with components of the extracellular matrix (ECM) can also impede the spread of liposomes to distant regions of the cancer tissue (82).

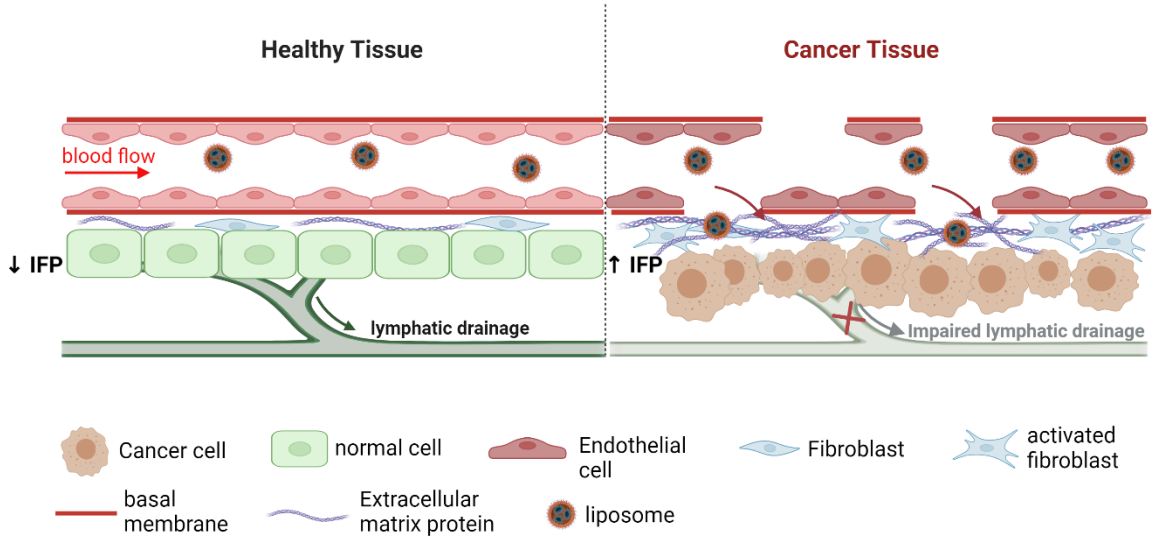

Figure 2. The principle of the EPR effect. In healthy tissues, the blood vessels are intact, which stops liposomes from passing the capillary wall. In contrast, cancer tissues have leaky blood vessels and poor lymphatic drainage, allowing liposomes to extravasate and accumulate. However, the deep penetration of these liposomes is obstructed by the high interstitial fluid pressure (IFP) and the dense extracellular matrix (ECM) (83, 84) (Created with BioRender.com).

1.3.3. Thermo-sensitive liposomal doxorubicin

Thermo-sensitive liposomes (TSLs) are spherical vesicles consisting of phospholipids that undergo a phase transition from a solid gel to a liquid-crystalline state at a temperature higher than the body's normal temperature, which is known as the melting phase transition temperature (Tm) (85). In the gel phase, the phospholipids remain well-arranged and immobile with fully extended hydrocarbon tails, maintaining the impermeability of the liposome membrane. As the temperature approaches the Tm, the phospholipid heads become mobile, causing a shift in the configuration of the C-C single bonds in the hydrocarbon chains from trans to gauche. This increase in the gauche conformers in the lipid hydrocarbon chains results in a loosening of the lipid packing (86). At this point, leaky and highly disordered microscopic regions start to form at the interface between the membrane domains that have become liquid and the ones that are still in the gel phase. Those permeable regions are called grain boundaries. The liposome membrane becomes completely fluid and permeable, facilitating the release of drugs at temperatures exceeding the Tm (Fig. 3 A) (67).

1,2-dipalmitoyl-sn-glycero-3-phosphocholine (DPPC) (Tm = 41.4 °C) is the main component in all TSL formulations, and is typically mixed with small amounts of phospholipids possessing a higher Tm, such as 1,2-distearoyl-sn-glycero-3-phosphocholine (DSPC) (Tm = 54.9 °C), to enhance the membrane stability (87). The combination of DPPC and DSPC was initially introduced as a TSL formulation by Yatvin et al. in 1978 and is currently known as traditional thermosensitive liposomes (TTSL) (Fig. 3 A). However, a notable limitation of this formulation was its slow and limited drug release rate (88). Thus, in more advanced TSL formulations the aim is to enhance drug release by modifying the lipid bilayer using lysolipids, synthetic polymers and phosphatidylglycerol lipids.

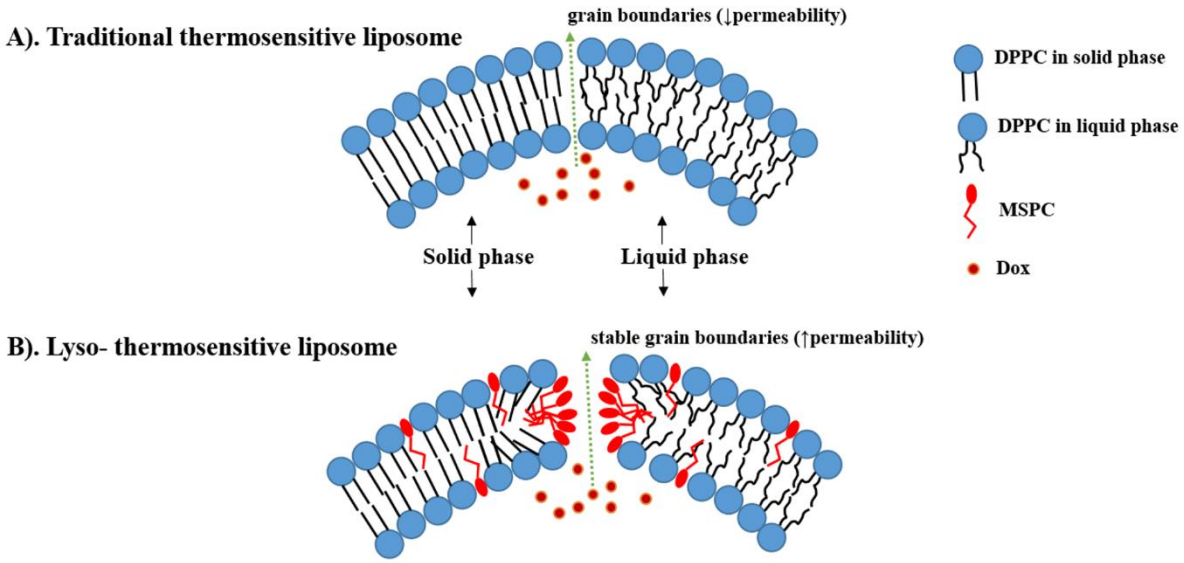

Figure 3. **The difference between traditional thermosensitive liposomes (TTSL) (A) and lyso-thermosensitive liposomal DOX (LTLD) (B) during the phase transition.** Lysolipids stabilize the grain boundaries, leading to a fast DOX release. Based on our review (67).

1.3.4. Lyso-thermosensitive liposomal doxorubicin (LTLD)

The prefix "lyso" refers to the removal of one of the two fatty acid chains in phospholipids through hydrolysis (89). As a result, lysolipids are small bioactive lipid molecules with only one acyl chain instead of two. Examples include mono-stearoyl-2-hydroxy-sn-

glycero-3-phosphocholine (MSPC) and mono-palmitoyl-2-hydroxy-sn-glycero-3-phosphocholine (MPPC) (90). Unlike DPPC and DSPC, which make up TTSL and contain two acyl chains, lysolipids have the 2-hydroxy-sn-glycero-3-PhosphoCholine complexed with just one stearoyl or palmitoyl residue (91).

Incorporating these shorter lysolipids into the TSL membrane significantly enhances the release of DOX. It is hypothesized that lysolipids accumulate in the grain boundaries, forming stable pores in the lipid bilayer during the phase transition. This phenomenon leads to increased membrane permeability and rapid release of DOX from the liposome at the heated tumor (approximately 80% of DOX released at 40–42 °C) (90, 92, 93) (Fig. 3B). This concept was initially introduced in 1999 by Needham, who incorporated 10% MPPC into PEGylated DPPC membranes of TTSL (DPPC:MPPC:DSPE-PEG-2000, molar ratio 90:10:4) (94). Subsequently, Needham et al. and Kong et al. assessed this formulation in mice with human squamous cell carcinoma xenografts (FaDu), demonstrating increased DOX accumulation in tumors and inhibition of tumor growth following treatment with LTLD at 42 °C compared to treatment with TTSL and non-TSL liposomes (NTSL) (94, 95)

In contrast to PLD, LTLD releases DOX directly into the bloodstream within the heated tumor, allowing DOX to diffuse from the blood vessels into the tumor interstitium (Fig. 4). This intravascular release strategy enhances DOX accumulation in the tumor and circumvents reliance on the EPR effect (96). A histological examination conducted by Manzoor et al. showed that treatment with LTLD combined with HT doubled the penetration of DOX compared to treatment with Doxil combined with HT (96).

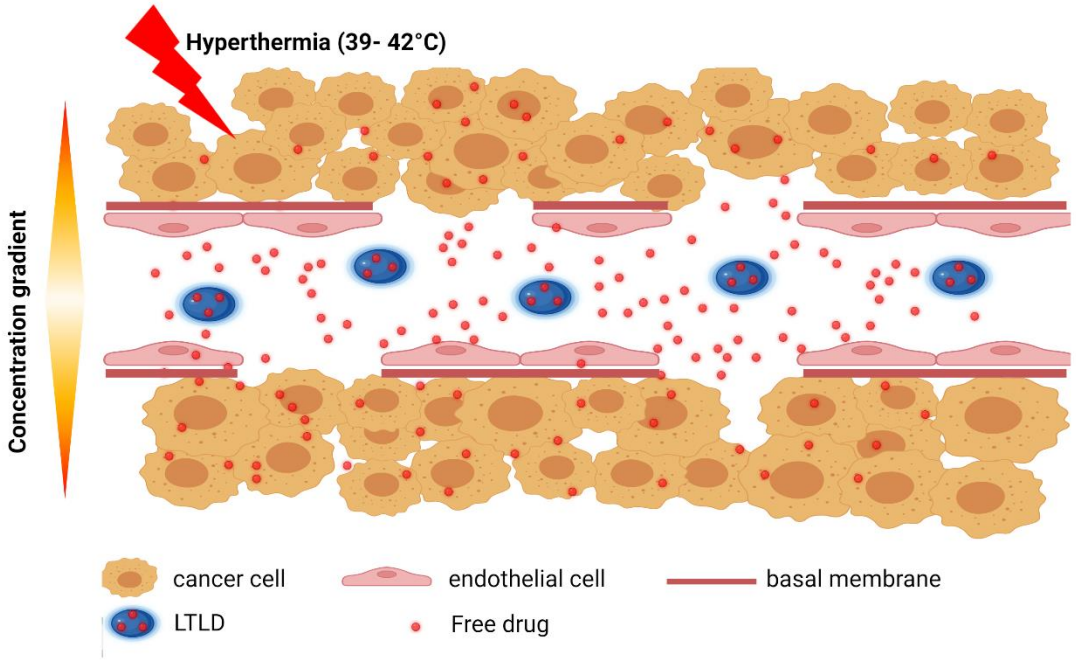

Figure 4. Principle of the lyso-thermosensitive liposomal doxorubicin (LTLD). LTLD releases DOX in the tumor's bloodstream when exposed to mild hyperthermia (39-42°C). The released DOX then diffuses from the blood vessels into the tumor interstitium, guided by the concentration gradient. Based on our review (83) "Created with Biorender.com".

Due to the short circulation time, the timing of LTLD administration (i.e., before or during HT) is critical for maximizing the potential clinical benefits. Previous preclinical studies have predominantly applied HT immediately after (97, 98) or shortly before LTLD administration (99, 100). Ponce et al. illustrated that tumor DOX levels doubled when LTLD was injected during HT compared to 15 minutes before HT (99). This enhancement in tumor DOX levels correlated with improved anti-cancer efficacy in rats with fibrosarcoma (99). Furthermore, LTLD infusion during HT led to a greater DOX accumulation in the bladder wall of pigs with bladder cancer compared to the combination of DOX and HT (101).

LTLD (Thermodox®, Celsion corporation) is the first TSL to reach clinical trial. Despite successful phase I trial (102), two phase III clinical trials (HEAT (103) and OPTIMA (104)), combining LTLD with radiofrequency ablation (RFA), did not meet the primary and secondary endpoints in hepatocellular carcinoma (HCC) patients. The lack of efficacy

in these phase III trials may be due to their similar design, which involved the same cancer type (HCC), single LTLD administration, and RFA to trigger DOX release (67, 105). Additionally, RFA causes heat diffusion from the ablative zone (T > 50°C) into the tumor margins (T: 39-40°C), where DOX is released from LTLD. An intermediate zone with vascular shunts can form between these regions, obstructing DOX delivery (106). This highlights the need to develop new HT modalities to activate LTLD effectively. The cancer-selective heating of mEHT might introduce it as a more efficient induction of DOX release from LTLD within the tumor.

1.4. Digoxin as an anti-cancer drug

Digoxin, a cardiac glycoside, serves as a medication for various heart problems such as congestive heart failure, and cardiac arrhythmias (107). Several studies have demonstrated anti-cancer effects of digoxin in different cancer models. These effects involved apoptosis induction (108, 109), proliferation inhibition (109, 110) and angiogenesis inhibition (108). Consequently, digoxin inhibited tumor growth in different cancer mouse models, including non-small cell lung cancer (111), and neuroblastoma (112), although such inhibitory effects were not observed after digoxin monotherapy in pancreatic (113), and prostate (114) cancer mouse models. Moreover, digoxin synergistically enhanced the efficacy of doxorubicin (115) and gemcitabine (113) *in vivo*. In TNBC, digoxin was demonstrated to induce apoptosis and reduce the proliferation of human TNBC cells *in vitro* (110). However, the *in vivo* efficacy of digoxin has not been investigated before in TNBC. Thus, in this study, we investigated the anti-cancer effects of digoxin in combination with mEHT.

2. Objectives

In the studies described in the present dissertation, we investigated the effects of mEHT on the delivery and efficacy of agents used in cancer therapy *in vivo*. In particular, we evaluated whether mEHT can:

- Enhance the cancer-specific delivery of DOX-encapsulated in lyso-thermosensitive liposomal doxorubicin (LTLD)
- Improve the cancer cell death of DOX-encapsulated in LTLD compared to free DOX and PEGylated liposomal doxorubicin (PLD)
- Augment apoptosis induction and proliferation inhibition of DOX-encapsulated in LTLD
- Synergistically enhance tumor growth inhibition by digoxin

3. Methods

3.1. Doxorubicin formulations

LTLD (Thermodox,) was provided by Celsion Cooperation (Lawrenceville, NJ, USA) in a frozen form. Each vial was filled with 15 ml of LTLD containing Doxorubicin hydrochloride at a concentration of 2 mg/ml. Post-thawing, the LTLD was portioned into 3 ml aliquots to prevent repeated freeze-thaw cycles and subsequently stored at -80°C. The PLD (Caelyx, 2 mg/ml) was supplied by Baxter Holdings (Utrecht, Netherlands). Prior to administration, both LTLD and PLD were diluted with 0.9% NaCl. Doxorubicin hydrochloride (MedChem Express, Monmouth Junction, USA, Cat. No. HY-15142) was dissolved in 0.9% NaCl to prepare a 1 mg/ml solution for use on treatment days.

3.2. Cell line

Murine 4T1 triple negative breast cancer (TNBC) cell line was obtained from Judy Lieberman (Lieberman Laboratory, Harvard University, Boston, MA, USA). 4T1 cells were grown in Dulbecco's Modified Essential Medium (DMEM) with 4.5 g/L glucose, but without L-glutamine and Phenol Red (Capricorn Scientific, Ebsdorfergrund, Germany, Cat. No. DMEM-HXRXA). The medium was supplemented with 10% Fetal Bovine Serum (FBS, South America Origen, EU approved, Eu-roClone S.p.A., Pero, Italy, Cat. No. ECS0180L), 10% Penicillin-Streptomycin mixture (Capricorn Scientific, Ebsdorfergrund, Germany, Cat. No. PS-B) and L-glutamine 200 mM (Capricorn Scientific, Ebsdorfergrund, Germany, Cat. No. GLN-B). The cells were kept at 37 °C in a humidified 5% CO2 incubator.

3.3. Animals

Female BALB/c mice aged six to eight weeks were housed under minimal disease (MD) conditions at the Animal Facility of the Basic Medical Science Center of Semmelweis University. Mice had unlimited access to tap water and standard mouse chow ad libitum and were kept on a 12-hour dark/light cycle. The housing and testing of the animals complied with Hungarian animal protection and welfare laws No. XXVIII/1998 and LXVII/2002, and with the directives of the European Union. All animal experiments received approval from the Pest County Government Office (PE/EA/50-2/2019).

3.4. mEHT treatment

Mice were treated with mEHT using a LabEHY 200 device (Oncotherm Kft., Budaörs, Hungary) (Fig. 5A), in accordance with the methods previously described (15, 19). The mEHT device produces an amplitude-modulated (AM), 13.56 MHz radiofrequency electromagnetic field through capacitive coupling between an adjustable upper electrode and a temperature-adjustable lower electrode. The lower electrode is connected to the mEHT device via a heating cable and radiofrequency (RF) cable (Fig. 5B), which allows for thermal regulation to maintain the mouse's body temperature within the physiological range during anaesthesia. In addition, the device is linked to a computer, enabling the adjustment of treatment parameters such as modulation, duration and power through the LabEHY software (Oncotherm Kft., Budaors, Hungary).

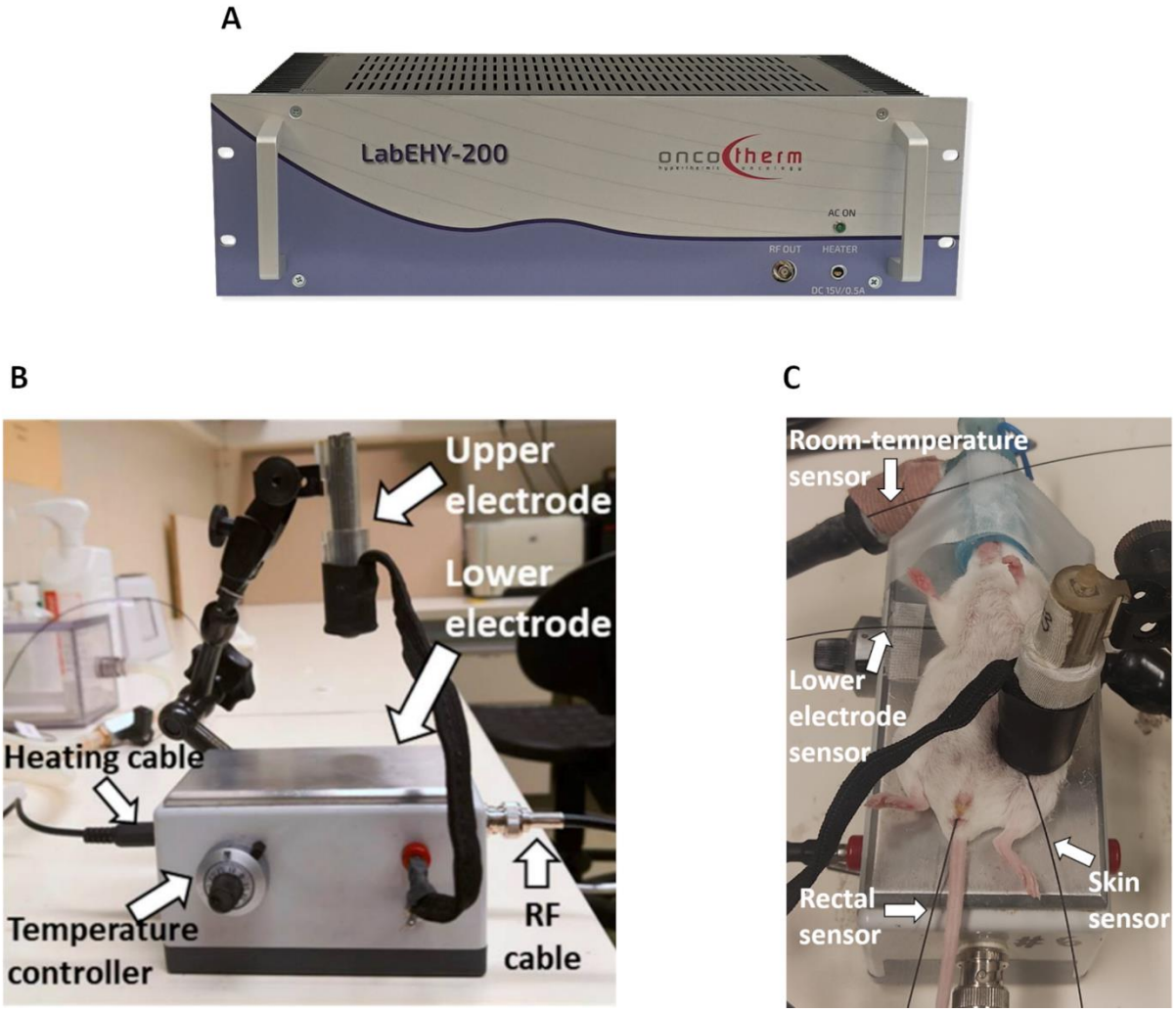

Figure 5. Modulated electro-hyperthermia (mEHT) treatment device for mice. (A) LabEHY 200 device. (B) Setup for mEHT treatment. (C) A mouse undergoing mEHT treatment (93).

Anesthesia of mice was induced with 5% isoflurane and maintained with 1.5–2% isoflurane. The mice were placed on the heating pad (i.e. the lower electrode), with the upper electrode fixed on the skin over the tumor. After a 3-minute warm-up period, the mice were treated with mEHT for 30 min at 0.7 ± 0.3 watts. Four temperature sensors were employed to record the temperature of the skin over the tumor, the rectum, the heating pad, and the room (Fig. 5C) (15, 19). During the treatment, the skin temperature was maintained at 40 °C, leading to a tumor temperature of 42.5 °C, as described earlier (15, 19). The temperatures of the rectum and the heating pad were 37 °C throughout the treatment.

3.5. Tumor growth inhibition study

Orthotopic breast tumors were induced in female BALB/c mice by subcutaneous injection of 1×10^6 4T1 cells in 50 μL Phosphate Buffered Saline (PBS) into the fat pad of the fourth mammary gland. The inoculation was performed under anesthesia with 5% isoflurane for induction and 1.5–2% isoflurane for maintenance. Eighth days after the implantation of 4T1 cells, tumor size was measured using ultrasound (US) and digital caliper as described earlier (15).

Three tumor growth inhibition studies were conducted. In the first study, we aimed to compare the effects of (mEHT+LTLD) to other DOX formulations. Therefore, on the 8th day after inoculation the mice were randomized into 7 groups according to tumor volume and body weight: sham+veh, sham+DOX, sham+PLD, mEHT+veh, mEHT+DOX, mEHT+PLD and mEHT+LTLD (n=5-6/group). The LTLD+sham group was omitted from this study because LTLD is not used in the clinic without hyperthermia (103, 116-118) (Table 1).

Table 1. Experimental Groups and number of mice per group

	mEHT	sham
vehicle (saline 0.9%)	5	5
free DOX	6	6
PLD	5	6
LTLD	5	-

Based on our pilot study results, we selected a 7.5 mg/kg dose of DOX for this study, out of the three previously tested doses (5, 7.5, and 10 mg/kg). In that pilot study, DOX at 10 mg/kg dose resulted in a 20% body weight loss, while the 5 mg/kg dose was ineffective in inhibiting tumor growth.

In the first study, we injected DOX, PLD and LTLD at a dosage of 7.5 mg/kg into the retro-orbital venous plexus, while the sham and mEHT groups were treated with equivalent volumes of 0.9% saline. Following findings from our pilot study, LTLD was slowly infused over a 3-minute period to prevent any potential hypersensitivity reactions. Immediately after drug administration, mEHT was performed for a duration of 30 minutes. The combined treatment was repeated three times at intervals of 72 hours (Fig. 6). Tumor volume and body weight were regularly monitored during the study. Body weight changes served as an indication of systemic toxicity. Euthanasia was performed 24 hours after the final treatment by cervical dislocation, and tumor tissues were excised. Half of each tumor specimen was kept in 4% formaldehyde solution (Molar Chemicals Ltd., Halásztelek, Hungary) for histological examination, while the remaining half was preserved in liquid nitrogen at -80 °C for subsequent molecular analysis.

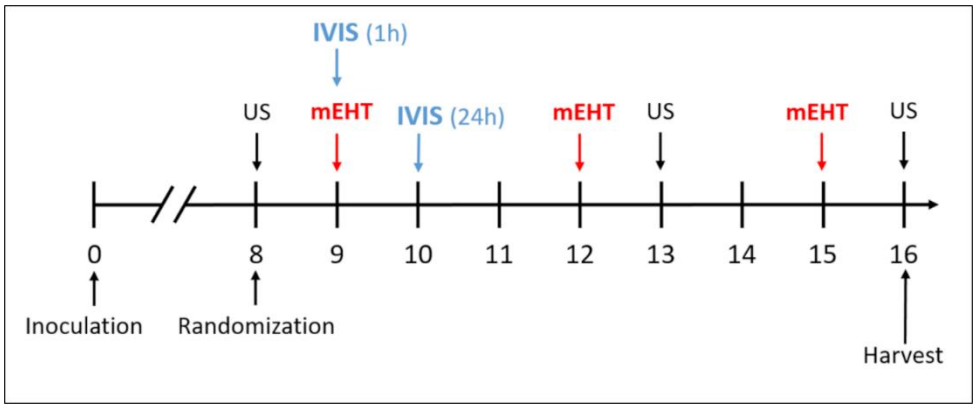

Figure 6. The schedule of the tumor growth inhibition study (93)**.**

In the second study, we monitored tumor growth for 5 days after the third mEHT treatment to determine the time at which the tumor stops shrinking. Mice were divided into three groups based on the results of the first experiment: sham+veh (n=5), mEHT+PLD (n=7), and mEHT+LTLD (n=9). We used the same experimental protocol as in the first study.

In the third study, we evaluated the effectiveness of combining mEHT with digoxin (Merck Life Science Kft., Cat. No. D6003). However, mice were treated with mEHT four times with a 48-h interval. Additionally, a daily intraperitoneal injection of digoxin at a dose of 2 mg/kg was given. Mice in the mEHT and sham groups were given equivalent volumes of saline. Digital caliper was used to evaluate the tumor size.

3.6. In vivo optical imaging of DOX accumulation in the cancer tissue

DOX accumulation in the cancer tissue was tracked by an *in vivo* imaging system (IVIS® Lumina XRMS Series III Imaging System, PerkinElmer). Mice (n=3) injected with 7.5 mg/kg DOX, PLD, and LTLD, with or without mEHT, underwent imaging at 1 and 24 hours after the treatment. The fluorescence signal of DOX was excited at 620 nm and captured at 500 nm using emission filters. Spectral unmixing method was applied to eliminate the autofluorescence background. The captured images were analysed using Living Image® 4.5 Software (PerkinElmer, Inc, Waltham, MA, USA). DOX fluorescence intensity was measured in efficiency units, defined as the ratio of detected emission radiance (photons (p)/second (s)/steradian (sr)/area(cm2) to excitation radiance (uW/cm2) (119). This efficiency unit was quantified in the tumor by delineating a region of interest (ROI) covering the tumor.

3.7. Histopathological analysis

Tumor samples were first fixed in 10% neutral-buffered formalin before embedding in paraffin. Formalin-fixed paraffin-embedded (FFPE) samples were then sectioned into 2.5 µm slices on a microtome at room temperature. The resulting serial sections were mounted onto glass slides and incubated in a thermostat (65°C for 1 hour). For

hematoxylin-eosin (H&E) staining, the tumor sections underwent deparaffinization and rehydration in xylene and descending concentrations of ethanol, respectively. After rehydration, the tumor sections were incubated with hematoxylin (#05-M06002, Bio Optica, Milano, Italy) for 10 minutes, blued for an additional 10 minutes, and incubated with eosin (#05-M10007, Bio Optica, Milano, Italy) for 5 minutes. The stained sections underwent dehydration using increasing concentrations of ethanol and xylene before being mounted with Bio Mount HM (#05-BMHM508, Bio Optica, Milano, Italy). Subsequently, the H&E-stained sections were scanned for further digital evaluation. Case Viewer image analysis software (3DHISTECH, Budapest, Hungary) was used to analyse the scanned images. The analysis was performed as described previously (120). Briefly, we distinguished damaged from viable areas under high digital magnification for each scanned tumor sample (Fig. 7). The Tumor Destruction Ratio (TDR) % was then calculated by dividing the damaged area by the total tumor area.

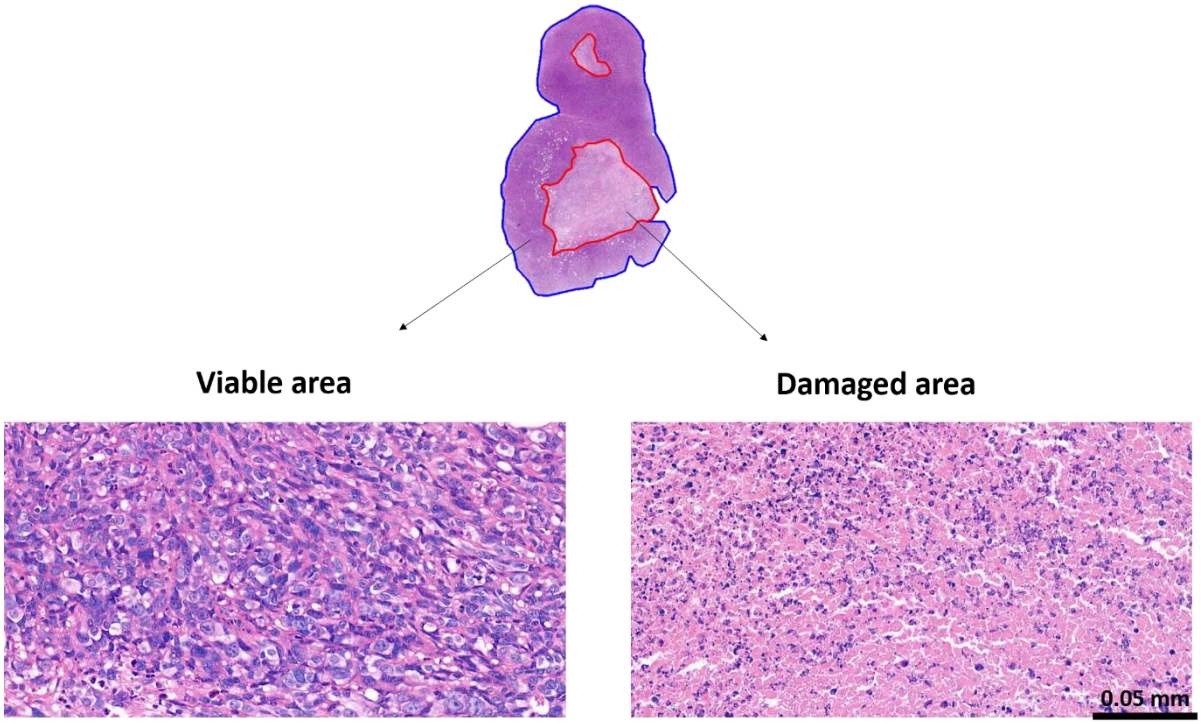

Figure 7. Comparison of damaged and viable tumor regions on hematoxylin-eosin-stained sections. Damaged area is circled in red, while the entire tumor area is circled in blue, with annotations indicating the distinction (93).

IHC for cleaved caspase3 (cC3) and Ki67 was conducted utilizing a polymer-peroxidase system (Histols, Histopathology Ltd., Pécs, Hungary), following previously established protocols (15). Briefly, tumor sections were deparaffinized, rehydrated, and treated with 3% H_2O_2 in methanol for 15 minutes to block endogenous peroxidases. Antigens were retrieved by incubating the slides in Tris–EDTA (TE) buffer pH 9.0 for 20 minutes in an Avair electric pressure cooker (ELLA 6 LUX, Bitalon Kft, Pécs, Hungary). 3% bovine serum albumin (BSA, #82-100-6, Millipore, Kankakee, Illinois, USA) was added for 20 min to block nonspecific protein binding. Tumor sections were then incubated with the diluted primary antibodies overnight at room temperature in a humidity chamber. Subsequently, the sections were incubated with peroxidase-conjugated secondary anti-rabbit and anti-mouse IgGs (HISTOLS-MR-T, micropolymer -30011.500T, Histopathology Ltd., Pécs, Hungary) for 40 minutes. The enzyme activity was detected under a microscope using a 3,3′-diaminobenzidine (DAB) chromogen/hydrogen peroxide kit (DAB Quanto-TA-060-QHDX-Thermo Fischer Scientific, Waltham, MA, USA). Finally, slides were scanned, and digitally assessed using the QuantCenter module of Case Viewer software by adjusting the intensity, color, and saturation within the annotated area. The expression of cC3 was evaluated across the entire tumor area and represented as the relative mask area (the ratio of the masked area to the whole annotated area). For Ki67 staining, the number of strongly Ki67+ nuclei were counted within the viable area. However, due to staining issues, data on Ki67 are unavailable for three samples. Table 2 provides a summary of the antibodies and dilutions utilized for IHC.

Table 2. Antibodies and dilutions utilized in immunohistochemistry (IHC) and western blot (WB)[1].

Antigen	type	reference.no	method	dilution	vendor[2]
cC3	rabbit, mAb	#9664	IHC	1:1600	Cell Signalling
			WB	1:1000	
Ki67	rabbit, mAb	#MA5-14520	IHC	1:50	Invitrogen
			WB	1:100	
β-actin	mouse, mAb	#ab6276	WB	1:5000	Abcam

[1]mAb: monoclonal antibody. cC3: cleaved caspase3, Ki67: proliferation marker, RRID: Research Resource Identifier. [2]Vendor specifications: Cell Signaling (Danvers, MA, USA), Invitrogen (Waltham, MA, USA), Abcam (Cambridge, MA, USA)

3.8. Western blot

Total protein was isolated from tumor samples using TRIzol reagent (Molecular Research Center lnc., Ohio, USA) following the manufacturer's instructions. Twenty micrograms of the isolated protein were loaded per well and separated on 12% SDS-PAGE. The separated proteins were transferred onto a polyvinylidene difluoride (PVDF) membrane (#1704156, Bio-Rad, Hercules, CA, USA). The membrane was cut into two strips to probe the same membrane for two proteins simultaneously. Blocking and antibody dilutions were performed in a Tris-buffered saline, supplemented with 5% skim milk and 0.05% Tween 20. The membrane was incubated with a primary antibody specific for cC3, Ki67 or β-actin overnight at 4 °C (Table 2). Following washing steps, the membrane was incubated with a horseradish peroxidase (HRP)-conjugated secondary antibody for an hour. Detection and visualization of the chemiluminescent signal was conducted by ECL Prime Western Blotting Detection Reagent (#RPN2232, Cytiva, MA, USA), and CHEMI Premium Imager (VWR, Radnor, PA, USA). The expression of proteins of interest was analysed by Image J software and normalised to β-actin.

3.9. Statistical analysis

The data are presented as mean ± SEM. Statistical analysis was performed using GraphPad Prism software (v.6.01; GraphPad Software, Inc., La Jolla, CA, USA). Two-way ANOVA followed by Tukey's post-hoc test was used to compare the changes in tumor volume, DOX accumulation in the tumor, and the body weight of the mice between groups. The normality of the data was assessed using the Kolmogorov–Smirnov test, and the homogeneity of variances in the groups was assessed using Bartlett's test. Since the data were normally distributed and variances of the groups were homogeneous, one-way ANOVA was used to compare tumor weights and expression of cC3 and Ki67 between the groups. The null hypothesis was rejected if * $p < 0.05$.

4. Results

4.1. mEHT improved tumor growth inhibition of DOX encapsulated in LTLD

Ultrasound and caliper recordings showed continuous tumor growth over time in the sham+vehicle-treated group (Figure 1A, B), leading to the heaviest tumors at the end of the observation period (Fig. 8C). While most treatments reduced tumor growth compared to the sham+vehicle group, mEHT+PLD- and mEHT+LTLD-treated mice carried the smallest tumors at the study's end (Fig. 8A, B).

Upon study termination, the largest tumors were observed in the sham+vehicle and sham+DOX groups. Tumors were smaller in the sham+PLD, mEHT+vehicle, and mEHT+DOX groups, while the smallest tumors were seen in the mEHT+PLD and mEHT+LTLD groups, as illustrated by the photos (Fig. 8D) and the tumor weight curve (Fig. 8C). Although mEHT+LTLD tumors were smaller than mEHT+PLD tumors (Fig. 8D), this difference was not statistically significant (Fig. 8C). However, mEHT+LTLD was the only treatment to reduce tumor weight significantly as compared to mEHT+DOX (Fig. 8C)

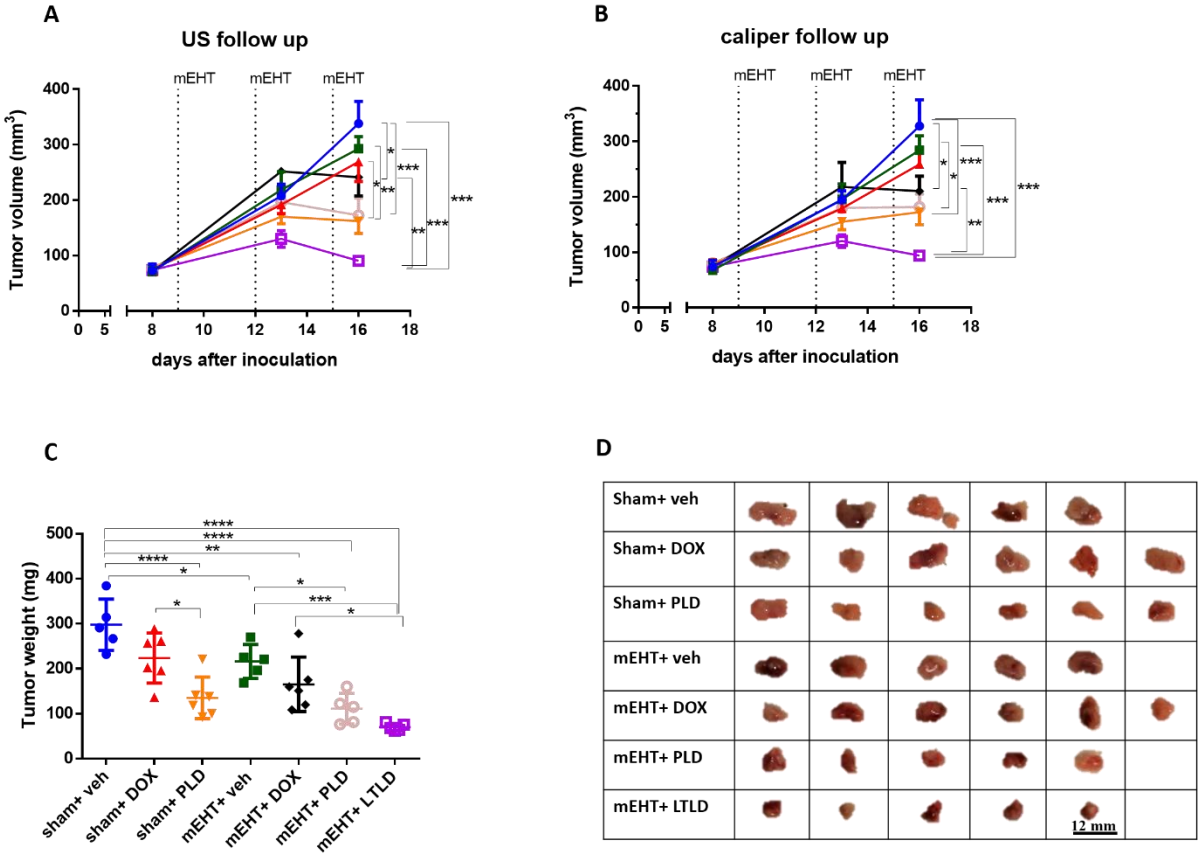

Figure 8. The impact of different treatments on tumor growth in 4T1-tumor bearing mice. mEHT: modulated electro hyperthermia, DOX: doxorubicin, PLD: PEGylated liposomal DOX, LTLD: lyso-thermosensitive liposomal DOX. (A) Ultrasound (US) and (B) digital caliper data following three mEHT treatments (indicated by dotted lines). (C) Tumor weight. Data are presented as mean±SEM. (D) Pictures of all excised tumors. Each row displays all tumors in that respective group. (A, B) Two-way ANOVA followed by Tukey's post hoc test, (C) one-way ANOVA followed by Tukey's post hoc test, n= 5-6/group, *: $p < 0.05$, **: $p < 0.01$, ***: $p < 0.001$, ****: $p < 0.0001$ (93).

In the second study, we investigated the tumor growth inhibitory effects of PLD and LTLD for 5 days after three mEHT-treatments. Notably, mEHT+LTLD exhibited significantly superior efficacy in inhibiting tumor growth compared to mEHT+PLD (Fig. 9A, B, C). Based on the ultrasound measurements, this difference was already significant after two treatments (Fig. 9A). Tumors subjected to either mEHT+LTLD or mEHT+PLD stopped growing after the second treatment and showed no signs of growth during the 5-day observation period after the last treatment (Fig. 9A). At the end of the study, tumors

treated with mEHT+LTLD were smaller compared to those treated with mEHT+PLD (Fig. 9B, C).

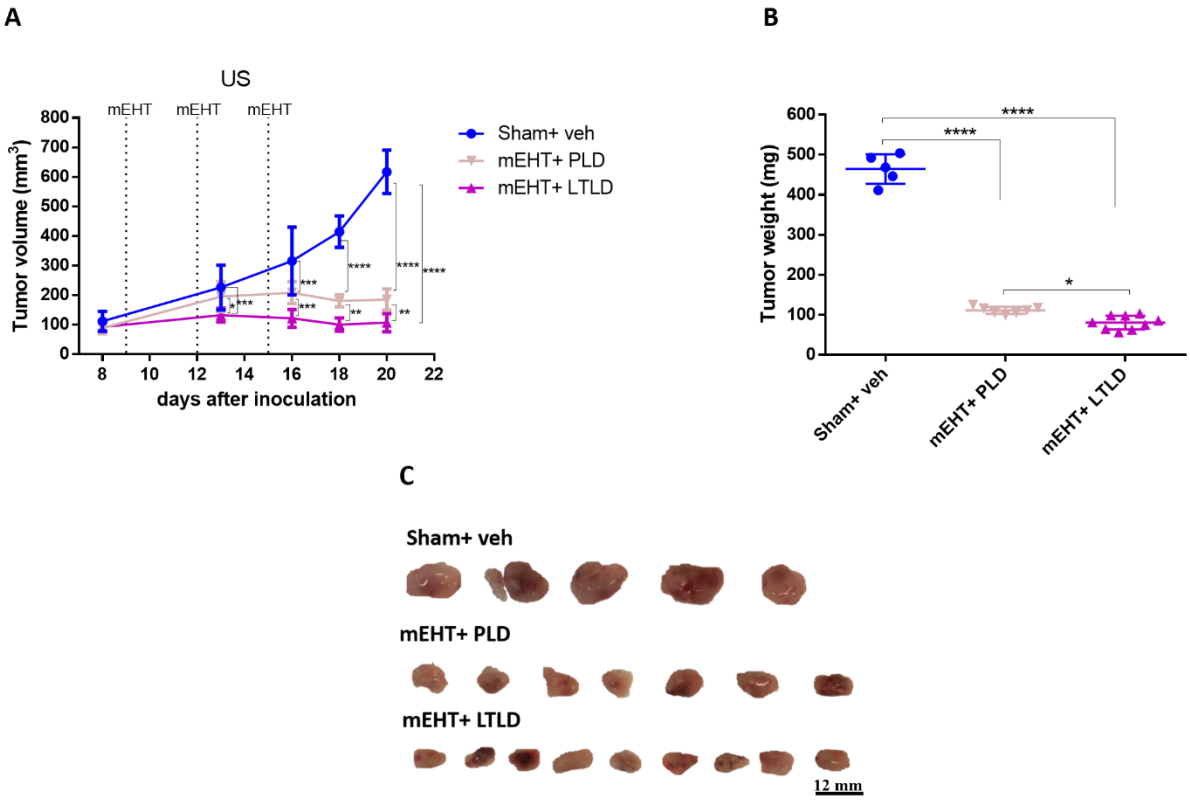

Figure 9. Effects of PLD and LTLD on tumor growth during a 5-day follow-up after treatment cessation in 4T1-tumor bearing mice. (A) Ultrasound (US) results. (B) Tumor weight. (C) Pictures of all excised tumors. Each row displays all tumors in that respective group. Data are presented as mean ± SEM, (A) two-way ANOVA followed by Tukey's post hoc test, (B) one-way ANOVA followed by Tukey's post hoc test, n= 5-9/ group, *: $p < 0.05$, **: $p < 0.01$, ***: $p < 0.001$, ****: $p < 0.0001$ (93).

4.2. mEHT accelerated the cancer tissue accumulation of DOX encapsulated in LTLD

One hour after the treatments, the *in vivo* imaging system (IVIS) did not show any DOX fluorescence signal in tumors treated with sham+DOX, sham+PLD, mEHT+DOX, and mEHT+PLD. Conversely, a strong DOX fluorescence signal was observed in tumors treated with mEHT+LTLD, indicating the highest accumulation of DOX in the tumors in the mEHT+LTLD group already at one hour. After 24 h, a 30% reduction was detected

in the DOX fluorescence signal in tumors treated with LTLD+mEHT. At this time point, PLD-treated and mEHT+PLD-treated tumors also exhibited DOX autofluorescence, comparable to LTLD-treated tumors (not significant) (Fig. 10 A, B.).

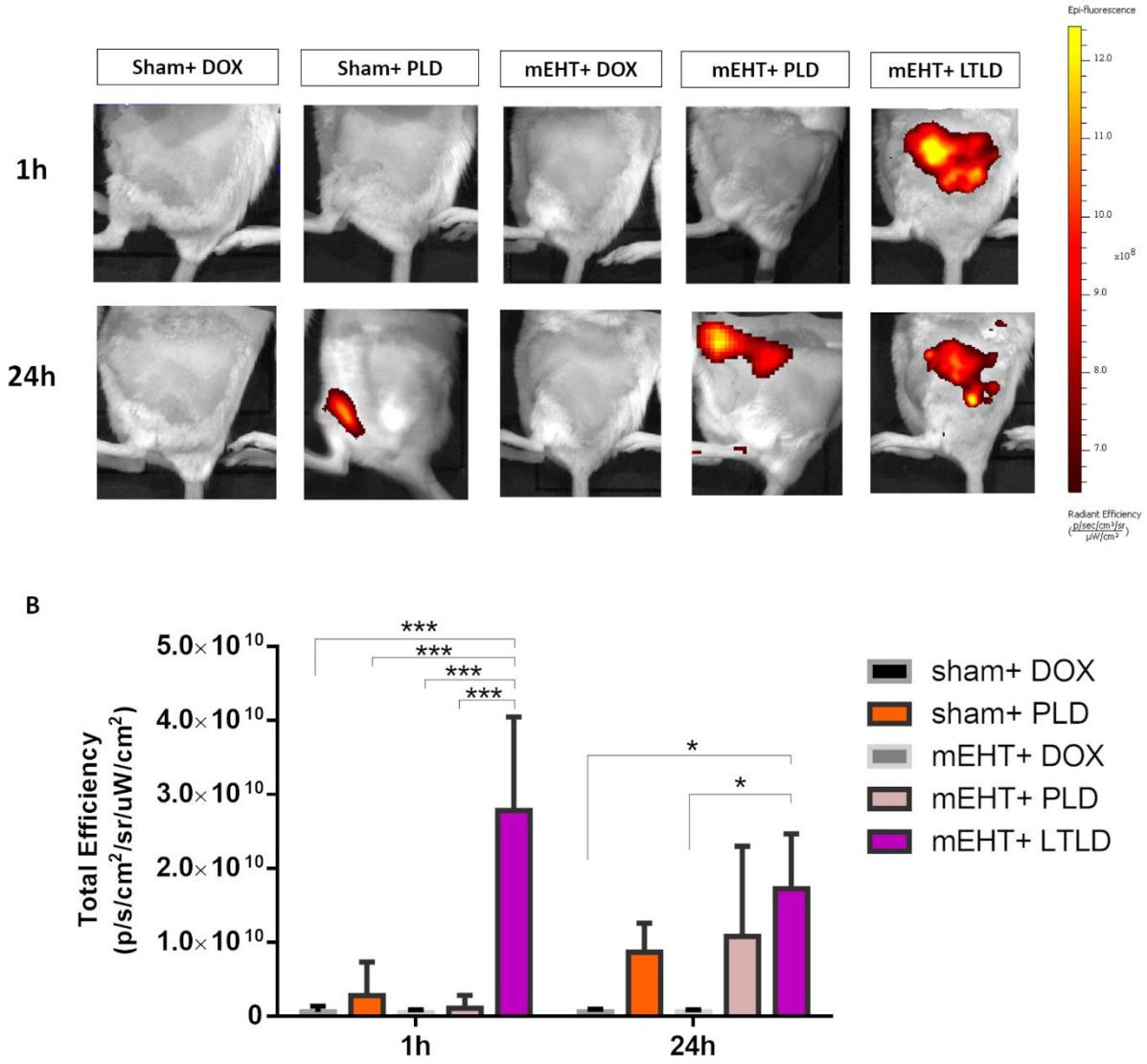

Figure 10. IVIS images illustrating DOX accumulation in cancer tissues at 1 and 24 hours after treatments in 4T1-tumor bearing mice. (A) Optical images of mice (DOX fluorescence signal depicted in yellow and red colors). (B) Quantification of DOX fluorescence intensity as total efficiency. Data are presented as mean ± SEM, Two-way ANOVA followed by Tukey's post hoc test, n= 3/ group, * $p < 0.05$, ** $p < 0.01$ and *** $p < 0.001$ (93).

4.3. mEHT+LTLD augmented the cancer tissue damage

Cancer cell damage was estimated on H&E-stained tumor sections by calculating the TDR. TDR was calculated by dividing the damaged area by the whole tumor area and expressed as %. The damaged tumor tissue was paler than the viable tissue on H&E-stained tumor sections. Small, damaged areas were observed in sham+vehicle- and sham+DOX-treated tumors. mEHT significantly increased the TDR compared to sham+vehicle, sham+DOX and sham+PLD groups. TDR was significantly higher in the PLD-treated group than in the sham+DOX group. Moreover, mEHT+PLD increased the TDR compared to PLD alone. TDR was significantly higher in the mEHT+LTLD group than in all other groups except the mEHT+PLD group. Although there was a small difference, mEHT+LTLD did not result in a significantly different TDR compared to mEHT+PLD (Fig. 11A, B).

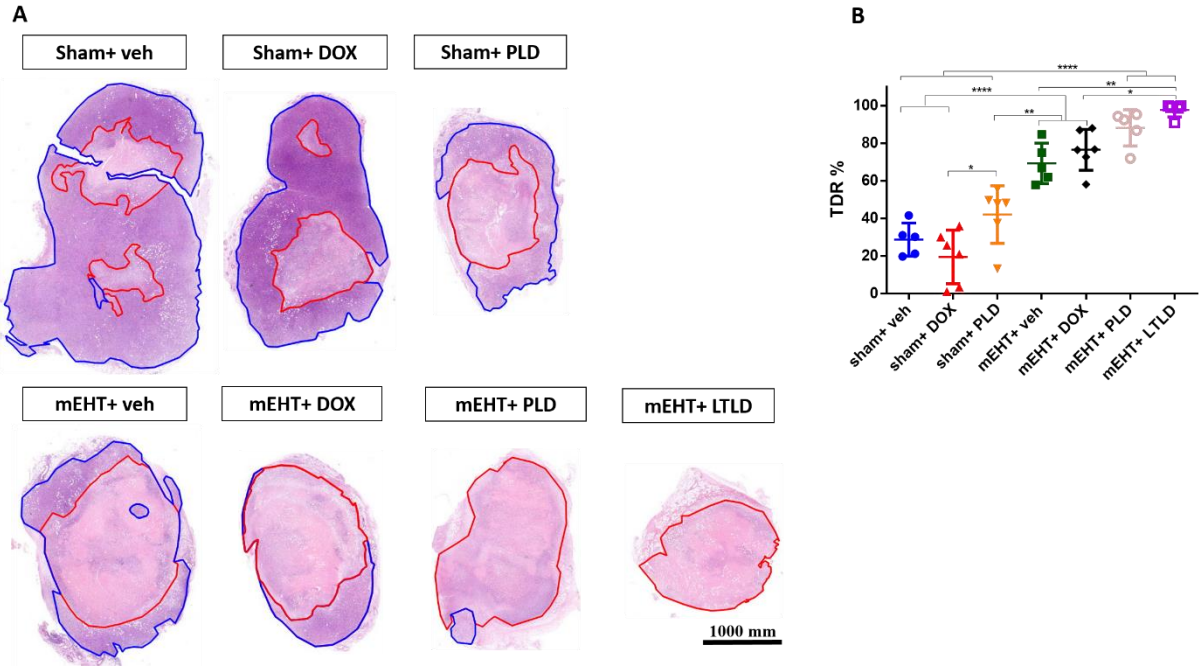

Figure 11. Tumor destruction ratio (TDR) at 24 h after the third mEHT treatment. (A) Viable (blue) and damaged (red) areas are evaluated on hematoxylin-eosin-stained sections. (B) TDR (%) is presented as the percentage of damaged area relative to the whole tumor area on hematoxylin and eosin-stained sections. Data are presented as mean±SEM, (B) one-way ANOVA followed by Tukey's post hoc test. n= 5-6/ group, *: $p < 0.05$, **: $p < 0.01$, ***: $p < 0.001$, ****: $p < 0.0001$ (93).

4.4. mEHT+LTLD enhanced caspase-dependent apoptosis

Apoptosis was evaluated 24 h after the last treatment by measuring cC3 expression in tumor tissues using IHC and western blot. The cC3 staining appeared dark brown on the IHC-stained tumors. The degree of cC3 staining significantly correlated with the TDR ($R2= 0.73$, $p < 0.0001$) (Fig. 12C), indicating the involvement of apoptosis in cell death. Sham+vehicle-treated tumors had small cC3-positive areas, demonstrating the lack of significant apoptosis. DOX or PLD did not induce a significant increase in cC3 staining compared to sham+vehicle. In contrast, mEHT-treated tumors had larger cC3-positive areas than tumors treated with sham or DOX alone. Combining mEHT with DOX or PLD did not increase the degree of cC3 staining. However, cC3 staining was the most intensive in mEHT+LTLD-treated tumors (Fig. 12A, B). Similarly, western blot demonstrated the strongest cC3 protein expression in mEHT+LTLD-treated tumors (Fig. 12 D, E).

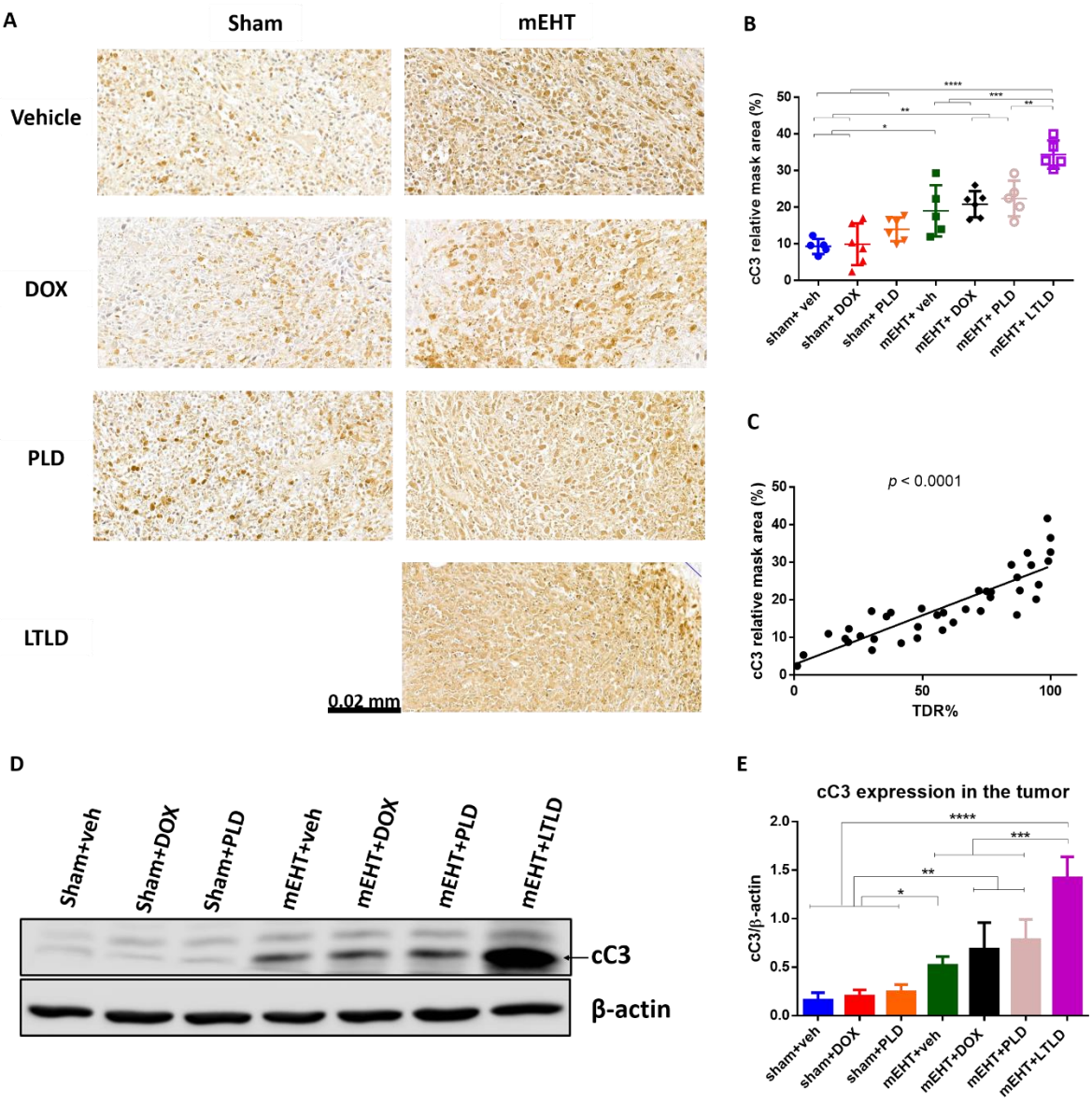

Figure 12. Expression of cleaved caspase3 (cC3) 24 h after the third mEHT treatment. (A) Representative cC3-immunostained sections at 42x magnification, with cC3-positive tumor cells appearing brown. (B) Quantification of relative cC3 staining in the tumors. (C) Correlation between cC3-stained area and TDR (%). (D) Representative images of western blot. (E) Quantification of cC3 levels by western blot. Data are presented as Mean ± SEM, (B, E) one-way ANOVA followed by Tukey's post hoc test. (C) Linear regression, n=5-6/ group, *: $p < 0.05$, **: $p < 0.01$, ***: $p < 0.001$, ****: $p < 0.0001$ (93).

4.5. mEHT+LTLD mitigated cancer cell proliferation

The proliferation of cancer cells was studied by evaluating the expression of Ki67 proliferation marker in the tumor at 24 h after the last treatment using IHC and western blot. Ki67-positive (Ki67+) nuclei were stained brown in the viable areas of the tumor. The highest number of Ki67+ nuclei was in the (sham+vehicle)-treated tumors. DOX and PLD did not reduce the number of Ki67+ nuclei as compared to sham+vehicle. However, mEHT significantly reduced the number of Ki67+ nuclei compared to tumors treated with sham+vehicle. The number of Ki67+ nuclei was significantly lower in (mEHT+DOX)-treated tumors compared to those treated with mEHT or DOX alone. The proliferation inhibition was further improved in (mEHT+PLD)-treated tumors. However, tumors in the (mEHT+LTLD) group had significantly fewer Ki67+ nuclei than tumors in all other groups (Fig. 13A, B). In line with the IHC findings, western blotting analysis of Ki67 revealed the lowest Ki67 expression in tumors treated with mEHT+LTLD (Fig. 13 C, D).

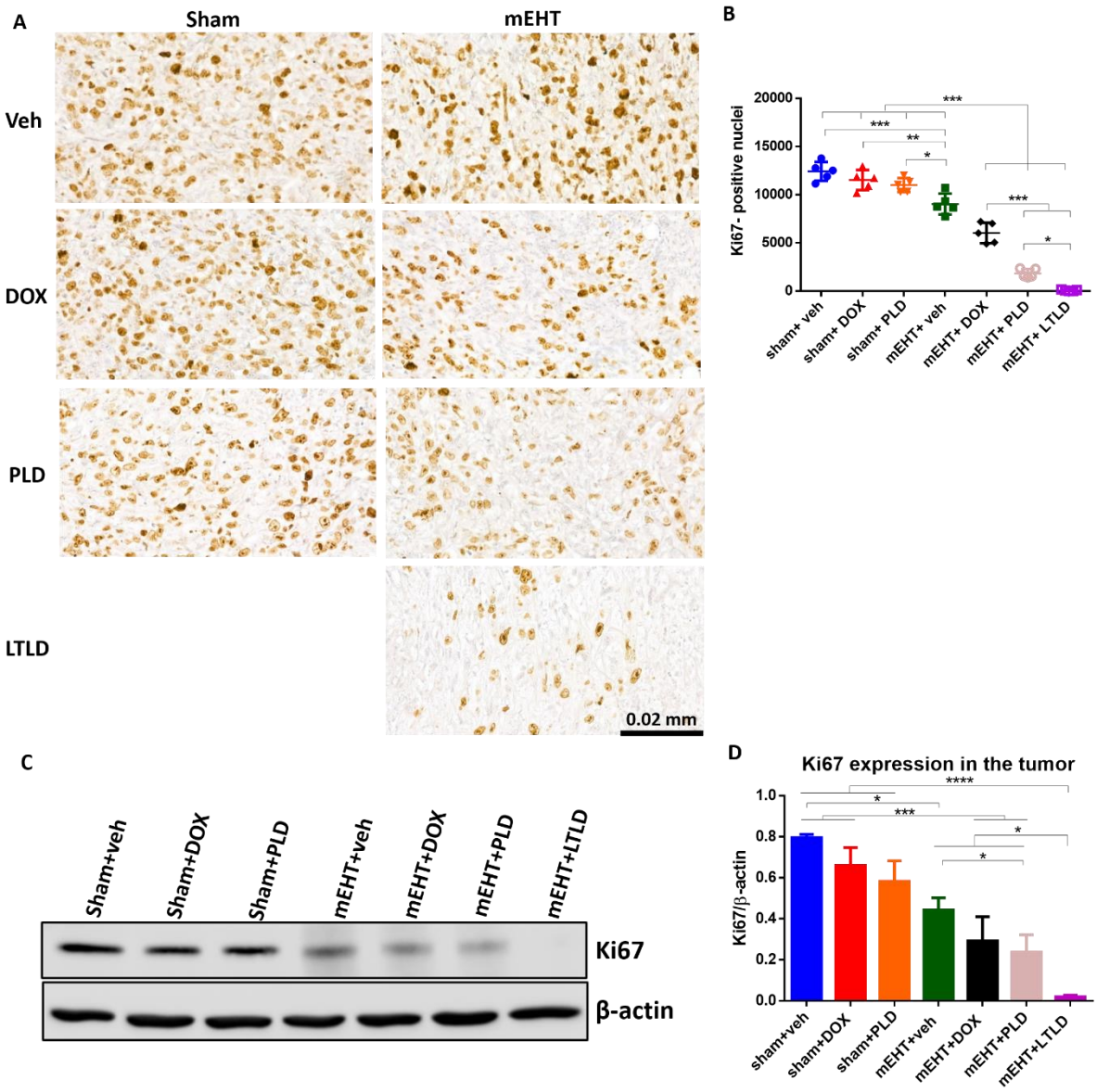

Figure 13. Effect of various treatments on cancer cell proliferation 24 h after the third mEHT treatment. (A) Representative images of Ki67-immunostained sections at 45x magnification. Ki67+ nuclei were stained brown and counted in the viable tumor area. (B) The number of Ki67+ nuclei. (C) Representative images of western blot. (D) Quantification of Ki67 levels by western blotting. Data are presented as mean ± SEM, (B, D) one-way ANOVA followed by Tukey's post hoc test. n= 5/group, *: $p < 0.05$, **: $p < 0.01$, ***: $p < 0.001$, ****: $p < 0.0001$ (93).

4.6. All DOX formulations reduced body weight

Mice treated with either Sham+vehicle or mEHT+vehicle maintained steady body weight throughout the study. Conversely, all mice treated with any form of DOX (DOX, PLD, or LTLD) showed a significant decrease in body weight (Fig. 14). These groups had similar patterns of body weight loss, and no significant differences were observed in the kinetics of weight loss (Fig. 14).

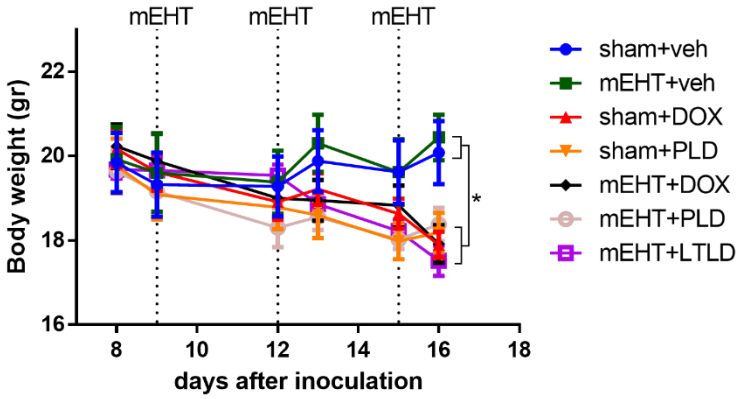

Figure 14. Body weight changes in 4T1-bearing mice subjected to different treatments. Data are presented as mean ± SEM, -Two-way ANOVA followed by Tuckey's post hoc test, n= 5-6/ group, *: $p < 0.05$, **: $p < 0.01$, ***: $p < 0.001$, ****: $p < 0.0001$ (93).

4.7. mEHT+Digoxin augmented cancer cell death

Tumor volume increased constantly in sham+saline-treated mice. Digoxin monotherapy did not influence tumor volume during or at the end of the study compared to the sham+saline group. Although mEHT-treated tumors were smaller than sham-treated tumors, this difference was not significant. By the end of the study, mEHT+digoxin resulted in the smallest tumors (Fig. 15 A).

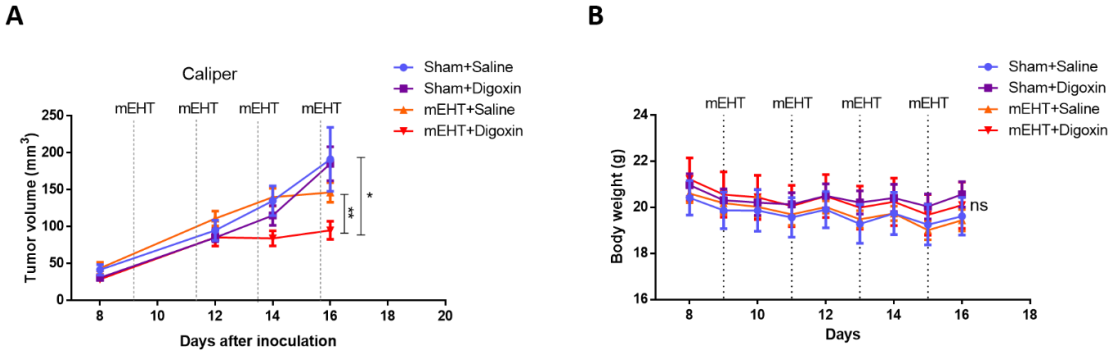

Figure 15. Effect of mEHT and digoxin on tumor growth and body weight in 4T1-bearing mice. (A) Tumor volume measured by digital caliper. (B) Body weight change. Data are presented as mean ± SEM, (A, B) Two-way ANOVA followed by Tuckey's post hoc test, n = 6–8/group; ns: not significant, *p < 0.05, **p < 0.01 (121).

Body weight was not reduced significantly in any of the digoxin study groups, suggesting the lack of toxicity. The body weight loss did not exceed 5 % in any of the groups. By the end of the study, there was no significant difference in body weight loss between the groups (Fig. 15 B).

5. Discussion

In the studies described in the present dissertation, we investigated whether modulated electro-hyperthermia (mEHT) can synergistically improve the anti-cancer activity of agents used in cancer therapy such as doxorubicin (DOX) and digoxin. A triple-negative breast cancer (TNBC) mouse model was chosen to test the effects of mEHT in combination with DOX or digoxin due to the aggressive nature and the limited treatment options in this cancer type.

In the present studies, we assessed the tumor accumulation and *in vivo* efficacy of DOX encapsulated in lyso-thermosensitive liposomes (LTLD) in mice subjected to mEHT, comparing the effects with other DOX formulations. In previous studies, DOX release from LTLD was induced by different conventional hyperthermia (cHT) methods, such as water bath in mice (122), or RFA in pigs (123) and humans (103). However, the anti-cancer effects of cHT primarily rely on the thermal effect, demonstrating only 1 °C ΔT between the tumor and surrounding tissues, which may not be sufficient to achieve sufficient DOX accumulation in cancer (29). On the other hand, mEHT possesses both thermal and non-thermal effects, achieving a ΔT of 2.5 °C (15). This renders the anticancer efficacy of mEHT superior to cHT (124, 125). In addition, the greater ΔT may facilitate enhanced local release of DOX from LTLD within the tumor. Due to its non-thermal effect and higher ΔT, mEHT's anti-cancer effect is more targeted, potentially reducing heat-related toxicities such as burns, frequently encountered after cHT (126). A review (127) proposed that mEHT can be used to activate thermosensitive liposomes (TSL). However, to date, no study has been conducted to explore this hypothesis.

Our studies revealed that treatment with mEHT+LTLD inhibits tumor growth the most. Notably, mEHT+LTLD demonstrated a significant reduction in tumor growth even after the second treatment similarly to mEHT+PLD. Consistent with our findings, Needham et al. showed that LTLD resulted in greater tumor growth reduction than PLD when both were combined with water bath in a human tumor xenograft model (122). Moreover, Dromi et al. demonstrated superior inhibition of tumor growth with LTLD compared to free DOX and PLD when pulsed high-intensity focused ultrasound (pulsed-HIFU) was used to heat the tumor(128). In pulsed-HIFU, short bursts of HIFU are applied to the

tumor, resulting in a small temperature elevation (39-44℃) (129). However, Wang et al. exhibited that while pulsed-HIFU raised the temperature of the tumor to 44℃, the surrounding muscles were warmed up to 42℃ (130). This can potentially result in a significant release of DOX from LTLD in the surrounding tissues.

In our studies, the enhanced inhibition of tumor growth observed in mice treated with mEHT+LTLD compared to mEHT+PLD is explained by the acceleration of DOX tumor delivery. A large accumulation of DOX in tumors was obtained one hour after mEHT+LTLD treatment, which is consistent with the pharmacokinetic profile of LTLD (90). Unlike PLD, LTLD does not rely on the EPR effect. LTLD releases approximately 80% of DOX directly into the bloodstream within the heated tumor, with subsequent diffusion of DOX into the tumor interstitium (90, 131). In contrast, PLD extravasation is predominantly dependent on the slow EPR effect (71). This difference in pharmacokinetics elucidates the improvement in early accumulation of DOX in the tumor when delivered via LTLD, but not when using PLD. Furthermore, this exclusive reliance of PLD on the EPR effect accounts for the enhanced DOX accumulation observed in tumors 24 hours after PLD administration (71). The decrease in tumor DOX accumulation was expected after 24 hours of LTLD treatment, which can be attributed to the wash-out of free DOX (132). These findings align with results from prior studies using LTLD in mice (97, 133).

Our findings revealed that mEHT did not augment PLD-derived DOX accumulation in the tumor, contrary to what was demonstrated in previous studies with a similar degree of hyperthermia (42°C) (128, 134). However, Tsang et al. showed that mEHT administered four hours after PLD-treatment could improve the cellular uptake of DOX, whereas we performed mEHT immediately after PLD administration (135). Hence, the timing of HT can influence cellular DOX uptake from PLD or LTLD.

Our histopathological analysis revealed that the greatest cancer damage was observed in tumors treated with mEHT+PLD or mEHT+LTLD, likely attributed to the synergistic effects of mEHT and DOX in promoting apoptosis. Previous studies by our group have demonstrated that mEHT induces caspase-dependent apoptosis (19). In the present study,

low levels of cC3 were observed in tumors treated with DOX alone. However, cC3 expression increased significantly when various DOX formulations were combined with mEHT, with the highest levels seen in the mEHT+LTLD group. This finding aligns with the results of Maswadeh et al., who demonstrated that TSL+HT improved apoptosis induction in murine fibrosarcoma compared to non-TSL+HT (136). Moreover, an *in vitro* study showed that PLD was more effective than free DOX in inducing apoptosis in oral squamous cell carcinoma CAL-27 cells. However, the effect of TSL was not evaluated (137). In this study, we did not explore other cell death mechanisms like necrosis or autophagy. Previously, we found that mEHT did not influence the gene expression of autophagy-related molecules such as Beclin1, autophagy-related protein 3 (ATG 5), ATG 3, and sequestosome 1 (SQSTM1).(19). In addition, necrosis is primarily activated by hyperthermia at temperatures above 45°C (138, 139).

DOX inhibits cancer cell proliferation (140), although in the current study, neither free DOX nor PLD alone reduced proliferation. However, a significant inhibition of proliferation was obtained after combining DOX with mEHT, particularly with the liposomal formulations (LTLD and PLD). Moreover, LTLD inhibited cancer cell proliferation much more than PLD. A previous report found that combining PLD with HT inhibited proliferation more effectively than either HT or PLD in a 4T1 mouse model. However, that study did not investigate the effects of TSL (141).

The current study revealed a comparable reduction in body weight of mice subjected to treatment with DOX, PLD, or LTLD. The LTLD membrane contains 10% lysolipids, which can dissociate from the membrane due to their interaction with plasma proteins, resulting in DOX leakage at physiological temperatures (142, 143). Conversely, due to the favorable pharmacokinetics of PLD, systemic toxicity is reduced (71). However, in the present study, PLD led to notable weight reductions. Besse et al. revealed that mice treated with LTLD at doses of 5 and 10 mg/kg experienced higher weight loss compared to those treated with DOX and PLD. The maximum weight loss observed in that study after LTLD treatment was 7% (144). In our study, the higher toxicity of LTLD was attributed to multiple dose administration (3 doses), which differs from the majority of previous preclinical studies where LTLD was given as a single dose (97, 122, 128, 144-

147). We selected the repeated dosing in accordance with clinical practice, where chemotherapeutic drugs and mEHT are typically used in cycles. Moreover, single dosing of LTLD has been implicated in the failure of clinical trials (105). Consequently, in two ongoing clinical trials, LTLD is being administered in cycles (NCT03749850, NCT02536183).

The primary limitation to show the full efficacy of treatment with mEHT+LTLD was the strong anticancer effect of the comparator mEHT+PLD. Consequently, the potential for enhancing these effects with LTLD was limited. Nevertheless, combining thermosensitive liposomes with mEHT introduces a new, clinically significant alternative. In this strategy, the targeted delivery of the chemotherapeutic agent to the tumor is not dependent on the EPR, which is known to vary significantly within and between different tumor types (78). Additionally, certain tumor types, like metastatic liver cancer, prostate cancer and pancreatic cancer, exhibit inadequate EPR due to dense fibrous stroma and limited blood vessel supply, hindering the penetration of nanoparticles (79, 148).

In the current study, we also demonstrated that the combination of mEHT and digoxin had a stronger anti-cancer effect than mEHT or digoxin alone. Digoxin monotherapy did not achieve significant tumor growth inhibition. However, when digoxin was combined with mEHT, a significant tumor growth inhibition was observed eight days after the first treatment with digoxin. It is important to mention that in previous studies, digoxin was given over a period of 14 to 40 days, at the dose of 2 mg/kg per day. On average, digoxin needed about 14 days of treatment, alone or in combination with other anticancer agents, to achieve significant tumor growth inhibition (111-113, 115). Thus, mEHT accelerated the anticancer effects of digoxin. In our study, digoxin at 2 mg/kg did not cause any signs of toxicity, as shown by lack of body weight loss. In the clinic, digoxin dose is titrated to the serum digoxin level of 0.8 – 2 ng/ml (149).

6. Conclusions

The studies summarized in this thesis investigated the synergism between modulated electro-hyperthermia (mEHT) and anti-cancer therapeutics such as doxorubicin (DOX) and digoxin in a TNBC mouse model. We concluded that:

1. mEHT can be used as a source of hyperthermia to activate thermosensitive nanoparticles such as lyso-thermosensitive liposomal doxorubicin (LTLD)
2. mEHT+LTLD is a novel, EPR-independent approach for DOX delivery to the cancer
3. mEHT accelerates tumor delivery of DOX from LTLD-encapsulated DOX
4. mEHT augments cancer destruction induced by different formulations of DOX, especially LTLD
5. The synergism between mEHT and DOX is mediated by inducing apoptosis and inhibiting the proliferation of cancer cells
6. mEHT improves the anti-cancer effect of digoxin in vivo
7. mEHT+digoxin is a safe and novel treatment option for TNBC

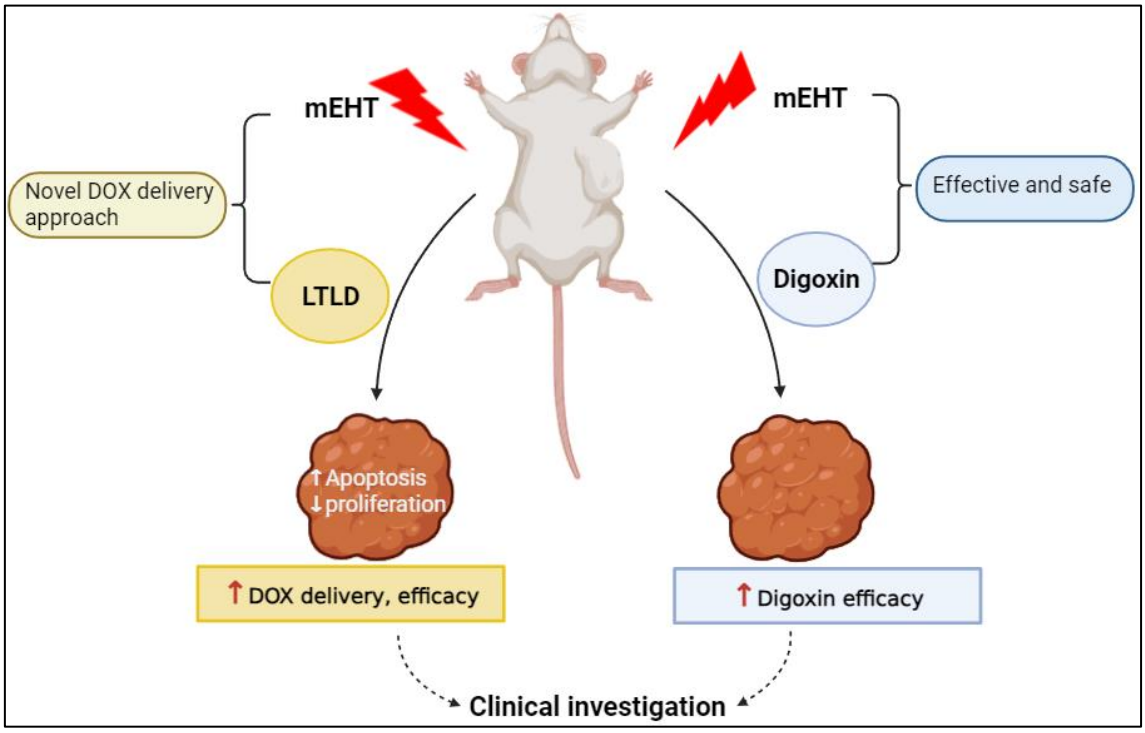

7. Summary

Triple-negative breast cancer (TNBC) is the most aggressive breast cancer subtype with limited treatment options. Modulated electro-hyperthermia (mEHT) is an adjuvant cancer therapy that enables tumor-selective heating (+2.5 °C). In this study, we investigated whether mEHT accelerates the tumor-specific delivery of doxorubicin (DOX) from lyso-thermosensitive liposomal doxorubicin (LTLD) and improves its anticancer efficacy in mice bearing a triple-negative breast cancer cell line (4T1). In addition, we explored if mEHT enhances the cancer cell death induced by digoxin.

The LTLD+mEHT combination was more effective at inhibiting tumor growth than free DOX or PLD, as demonstrated by reductions in both the tumor volume and tumor weight. LTLD+mEHT resulted in the highest DOX accumulation in the cancer tissue one hour after treatment. Cancer cell damage was associated with an increase in cC3 in the damaged area, and a reduction in Ki67 in the viable tumor. These changes were the strongest in the LTLD+mEHT-treated tumors. The body weight loss was similar in all mice treated with the various DOX formulation, suggesting no difference in toxicity. In another experiment, mEHT+digoxin combination exhibited stronger tumor inhibitory effects than mEHT or digoxin monotherapy, without signs of toxicity.

However, the results of these studies should be supported by further investigations on mEHT+LTLD and mEHT+digoxin in larger animals, such as pigs. As mEHT, LTLD, and digoxin are under clinical trials, the clinical investigation of these combinations in breast cancer patients is warranted.

8. Bibliography

1. Dass SA, Tan KL, Selva Rajan R, Mokhtar NF, Mohd Adzmi ER, Wan Abdul Rahman WF, Tengku Din T, Balakrishnan V. Triple Negative Breast Cancer: A Review of Present and Future Diagnostic Modalities. Medicina (Kaunas, Lithuania). 2021;57(1).

2. Griffiths CL, Olin JL. Triple Negative Breast Cancer: A Brief Review of its Characteristics and Treatment Options. Journal of Pharmacy Practice. 2012;25(3):319-323.

3. Brouckaert O, Wildiers H, Floris G, Neven P. Update on triple-negative breast cancer: prognosis and management strategies. International journal of women's health. 2012;4:511-520.

4. Bou Zerdan M, Ghorayeb T, Saliba F, Allam S, Bou Zerdan M, Yaghi M, Bilani N, Jaafar R, Nahleh Z. Triple Negative Breast Cancer: Updates on Classification and Treatment in 2021. Cancers. 2022;14(5).

5. Prat A, Parker JS, Karginova O, Fan C, Livasy C, Herschkowitz JI, He X, Perou CM. Phenotypic and molecular characterization of the claudin-low intrinsic subtype of breast cancer. Breast cancer research : BCR. 2010;12(5):R68.

6. Lee J. Current Treatment Landscape for Early Triple-Negative Breast Cancer (TNBC). Journal of clinical medicine. 2023;12(4).

7. Cortes J, Cescon DW, Rugo HS, Nowecki Z, Im SA, Yusof MM, Gallardo C, Lipatov O, Barrios CH, Holgado E, Iwata H, Masuda N, Otero MT, Gokmen E, Loi S, Guo Z, Zhao J, Aktan G, Karantza V, Schmid P. Pembrolizumab plus chemotherapy versus placebo plus chemotherapy for previously untreated locally recurrent inoperable or metastatic triple-negative breast cancer (KEYNOTE-355): a randomised, placebo-controlled, double-blind, phase 3 clinical trial. Lancet (London, England). 2020;396(10265):1817-1828.

8. Cortes J, Rugo HS, Cescon DW, Im SA, Yusof MM, Gallardo C, Lipatov O, Barrios CH, Perez-Garcia J, Iwata H, Masuda N, Torregroza Otero M, Gokmen E, Loi S, Guo Z, Zhou X, Karantza V, Pan W, Schmid P. Pembrolizumab plus Chemotherapy in Advanced Triple-Negative Breast Cancer. The New England journal of medicine. 2022;387(3):217-226.

9. Schmid P, Cortes J, Dent R, Pusztai L, McArthur H, Kümmel S, Bergh J, Denkert C, Park YH, Hui R, Harbeck N, Takahashi M, Untch M, Fasching PA, Cardoso F, Andersen

J, Patt D, Danso M, Ferreira M, Mouret-Reynier MA, Im SA, Ahn JH, Gion M, Baron-Hay S, Boileau JF, Ding Y, Tryfonidis K, Aktan G, Karantza V, O'Shaughnessy J. Event-free Survival with Pembrolizumab in Early Triple-Negative Breast Cancer. The New England journal of medicine. 2022;386(6):556-567.

10. Schmid P, Cortes J, Pusztai L, McArthur H, Kümmel S, Bergh J, Denkert C, Park YH, Hui R, Harbeck N, Takahashi M, Foukakis T, Fasching PA, Cardoso F, Untch M, Jia L, Karantza V, Zhao J, Aktan G, Dent R, O'Shaughnessy J. Pembrolizumab for Early Triple-Negative Breast Cancer. The New England journal of medicine. 2020;382(9):810-821.

11. Park MK, Lee CH, Lee H. Mouse models of breast cancer in preclinical research. Laboratory animal research. 2018;34(4):160-205.

12. Liu C, Wu P, Zhang A, Mao X. Advances in Rodent Models for Breast Cancer Formation, Progression, and Therapeutic Testing. Frontiers in oncology. 2021;11:593337.

13. Holen I, Saleh L, Ottewell PD, Lawson MA. Chapter 4 - In vivo models used in studies of bone metastases. In: Heymann D, editor. Bone Sarcomas and Bone Metastases - From Bench to Bedside (Third Edition): Academic Press; 2022. p. 35-53.

14. Pulaski BA, Ostrand-Rosenberg S. Mouse 4T1 Breast Tumor Model. Current Protocols in Immunology. 2000;39(1):20.2.1-.2.16.

15. Danics L, Schvarcz CA, Viana P, Vancsik T, Krenács T, Benyó Z, Kaucsár T, Hamar P. Exhaustion of Protective Heat Shock Response Induces Significant Tumor Damage by Apoptosis after Modulated Electro-Hyperthermia Treatment of Triple Negative Breast Cancer Isografts in Mice. Cancers (Basel). 2020;12(9).

16. Liu K, Paschall AV. An Orthotopic Mouse Model of Spontaneous Breast Cancer Metastasis. JoVE. 2016(114):e54040.

17. Tao K, Fang M, Alroy J, Sahagian GG. Imagable 4T1 model for the study of late stage breast cancer. BMC Cancer. 2008;8:228.

18. Pulaski BA, Ostrand-Rosenberg S. Reduction of established spontaneous mammary carcinoma metastases following immunotherapy with major histocompatibility complex class II and B7.1 cell-based tumor vaccines. Cancer Res. 1998;58(7):1486-1493.

19. Schvarcz CA, Danics L, Krenács T, Viana P, Béres R, Vancsik T, Nagy Á, Gyenesei A, Kun J, Fonović M, Vidmar R, Benyó Z, Kaucsár T, Hamar P. Modulated Electro-

Hyperthermia Induces a Prominent Local Stress Response and Growth Inhibition in Mouse Breast Cancer Isografts. Cancers (Basel). 2021;13(7).
20. Nagata T, Kanamori M, Sekine S, Arai M, Moriyama M, Fujii T. Clinical study of modulated electro-hyperthermia for advanced metastatic breast cancer. Molecular and clinical oncology. 2021;14(5):103.
21. Kim S, Lee JH, Cha J, You SH. Beneficial effects of modulated electro-hyperthermia during neoadjuvant treatment for locally advanced rectal cancer. International journal of hyperthermia : the official journal of European Society for Hyperthermic Oncology, North American Hyperthermia Group. 2021;38(1):144-151.
22. Fiorentini G, Sarti D, Casadei V, Milandri C, Dentico P, Mambrini A, Nani R, Fiorentini C, Guadagni S. Modulated Electro-Hyperthermia as Palliative Treatment for Pancreatic Cancer: A Retrospective Observational Study on 106 Patients. Integrative cancer therapies. 2019;18:1534735419878505.
23. Minnaar CA, Maposa I, Kotzen JA, Baeyens A. Effects of Modulated Electro-Hyperthermia (mEHT) on Two and Three Year Survival of Locally Advanced Cervical Cancer Patients. Cancers (Basel). 2022;14(3).
24. Fiorentini G, Sarti D, Mambrini A, Hammarberg Ferri I, Bonucci M, Sciacca PG, Ballerini M, Bonanno S, Milandri C, Nani R, Guadagni S, Dentico P, Fiorentini C. Hyperthermia combined with chemotherapy vs chemotherapy in patients with advanced pancreatic cancer: A multicenter retrospective observational comparative study. World journal of clinical oncology. 2023;14(6):215-226.
25. Vander Heiden MG, Cantley LC, Thompson CB. Understanding the Warburg effect: the metabolic requirements of cell proliferation. Science (New York, NY). 2009;324(5930):1029-1033.
26. Lee S-Y, Lorant G, Grand L, Szasz AM. The Clinical Validation of Modulated Electro-Hyperthermia (mEHT). Cancers. 2023; 15(18).
27. Griffiths H, Ahmed A, Smith CW, Moore JL, Kerby IJ, Davies RM. Specific absorption rate and tissue temperature in local hyperthermia. International journal of radiation oncology, biology, physics. 1986;12(11):1997-2002.
28. Viana P, Hamar P. Targeting the heat shock response induced by modulated electro-hyperthermia (mEHT) in cancer. Biochimica et Biophysica Acta (BBA) - Reviews on Cancer. 2024;1879(2):189069.

29. Roussakow S. The History of Hyperthermia Rise and Decline. Conference Papers in Medicine. 2013;2013:428027.
30. Alshaibi HF, Al-shehri B, Hassan B, Al-zahrani R, Assiss T. Modulated Electrohyperthermia: A New Hope for Cancer Patients. BioMed Research International. 2020;2020:8814878.
31. Andocs G, Szasz O, Szasz A. Oncothermia treatment of cancer: from the laboratory to clinic. Electromagnetic biology and medicine. 2009;28(2):148-165.
32. Krenacs T, Meggyeshazi N, Forika G, Kiss E, Hamar P, Szekely T, Vancsik T. Modulated Electro-Hyperthermia-Induced Tumor Damage Mechanisms Revealed in Cancer Models. Int J Mol Sci. 2020;21(17).
33. Lau WY, Lai ECH. The Current Role of Radiofrequency Ablation in the Management of Hepatocellular Carcinoma: A Systematic Review. Annals of Surgery. 2009;249(1).
34. Islam R, Maeda H, Fang J. Factors affecting the dynamics and heterogeneity of the EPR effect: pathophysiological and pathoanatomic features, drug formulations and physicochemical factors. Expert opinion on drug delivery. 2022;19(2):199-212.
35. Alimoradi H, Matikonda SS, Gamble AB, Giles GI, Greish K. Hypoxia Responsive Drug Delivery Systems in Tumor Therapy. Current pharmaceutical design. 2016;22(19):2808-2820.
36. Navi BB, Reiner AS, Kamel H, Iadecola C, Okin PM, Tagawa ST, Panageas KS, DeAngelis LM. Arterial thromboembolic events preceding the diagnosis of cancer in older persons. Blood. 2019;133(8):781-809.
37. Gillies RJ, Schornack PA, Secomb TW, Raghunand N. Causes and effects of heterogeneous perfusion in tumors. Neoplasia (New York, NY). 1999;1(3):197-207.
38. Tehrani MHH, Moradi Kashkooli F, Soltani M. Effect of tumor heterogeneity on enhancing drug delivery to vascularized tumors using thermo-sensitive liposomes triggered by hyperthermia: A multi-scale and multi-physics computational model. Computers in Biology and Medicine. 2024;170:108050.
39. Bicher HI, Hetzel FW, Sandhu TS, Frinak S, Vaupel P, O'Hara MD, O'Brien T. Effects of hyperthermia on normal and tumor microenvironment. Radiology. 1980;137(2):523-530.
40. Vaupel PW, Otte J, Manz R. Oxygenation of malignant tumors after localized microwave hyperthermia. Radiation and Environmental Biophysics. 1982;20(4):289-300.

41. Lee SY, Kim JH, Han YH, Cho DH. The effect of modulated electro-hyperthermia on temperature and blood flow in human cervical carcinoma. International journal of hyperthermia : the official journal of European Society for Hyperthermic Oncology, North American Hyperthermia Group. 2018;34(7):953-960.
42. Vancsik T, Forika G, Balogh A, Kiss E, Krenacs T. Modulated electro-hyperthermia induced p53 driven apoptosis and cell cycle arrest additively support doxorubicin chemotherapy of colorectal cancer in vitro. Cancer medicine. 2019;8(9):4292-4303.
43. Qin W, Akutsu Y, Andocs G, Suganami A, Hu X, Yusup G, Komatsu-Akimoto A, Hoshino I, Hanari N, Mori M, Isozaki Y, Akanuma N, Tamura Y, Matsubara H. Modulated electro-hyperthermia enhances dendritic cell therapy through an abscopal effect in mice. Oncology reports. 2014;32(6):2373-2409.
44. Lee SY, Lee NR, Cho DH, Kim JS. Treatment outcome analysis of chemotherapy combined with modulated electro-hyperthermia compared with chemotherapy alone for recurrent cervical cancer, following irradiation. Oncology letters. 2017;14(1):73-108.
45. Lee SY, Lee DH, Cho DH. Modulated electrohyperthermia in locally advanced cervical cancer: Results of an observational study of 95 patients. Medicine. 2023;102(3):e32727.
46. Iyikesici MS SA, Turkmen E, Akdemir O, Slocum AK, et al. . Complete Response of Locally Advanced (stage III) Rectal Cancer to Metabolically Supported Chemoradiotherapy with Hyperthermia. Int J Cancer Res Mol Mech. 2016;2.1.
47. Li Z, Sun Q, Huang X, Zhang J, Hao J, Li Y, Zhang S. The Efficacy of Radiofrequency Hyperthermia Combined with Chemotherapy in the Treatment of Advanced Ovarian Cancer. Open medicine (Warsaw, Poland). 2018;13:83-109.
48. Ranieri G, Laface C, Laforgia M, De Summa S, Porcelli M, Macina F, Ammendola M, Molinari P, Lauletta G, Di Palo A, Rubini G, Ferrari C, Gadaleta CD. Bevacizumab Plus FOLFOX-4 Combined With Deep Electro-Hyperthermia as First-line Therapy in Metastatic Colon Cancer: A Pilot Study. Frontiers in oncology. 2020;10:590707.
49. Arcamone F, Cassinelli G, Fantini G, Grein A, Orezzi P, Pol C, Spalla C. Adriamycin, 14-hydroxydaunomycin, a new antitumor antibiotic from S. peucetius var. caesius. Reprinted from Biotechnology and Bioengineering, Vol. XI, Issue 6, Pages 1101-1110 (1969). Biotechnology and bioengineering. 2000;67(6):704-713.

50. Prados J, Melguizo C, Ortiz R, Vélez C, Alvarez PJ, Arias JL, Ruíz MA, Gallardo V, Aranega A. Doxorubicin-loaded nanoparticles: new advances in breast cancer therapy. Anti-cancer agents in medicinal chemistry. 2012;12(9):1058-1070.
51. Sehouli J, Camara O, Schmidt M, Mahner S, Seipelt G, Otremba B, Schmalfeldt B, Tesch H, Lorenz-Schlüter C, Oskay-Ozcelik G. Pegylated liposomal doxorubicin (CAELYX) in patients with advanced ovarian cancer: results of a German multicenter observational study. Cancer chemotherapy and pharmacology. 2009;64(3):585-591.
52. Cross RJ, Glashan RW, Humphrey CS, Robinson RG, Smith PH, Williams RE. Treatment of advanced bladder cancer with adriamycin and 5-fluorouracil. British journal of urology. 1976;48(7):609-615.
53. Hong Y, Che S, Hui B, Yang Y, Wang X, Zhang X, Qiang Y, Ma H. Lung cancer therapy using doxorubicin and curcumin combination: Targeted prodrug based, pH sensitive nanomedicine. Biomedicine & pharmacotherapy = Biomedecine & pharmacotherapie. 2019;112:108614.
54. Tacar O, Sriamornsak P, Dass CR. Doxorubicin: an update on anticancer molecular action, toxicity and novel drug delivery systems. The Journal of pharmacy and pharmacology. 2013;65(2):157-170.
55. Thorn CF, Oshiro C, Marsh S, Hernandez-Boussard T, McLeod H, Klein TE, Altman RB. Doxorubicin pathways: pharmacodynamics and adverse effects. Pharmacogenetics and genomics. 2011;21(7):440-506.
56. Kciuk M, Gielecińska A, Mujwar S, Kołat D, Kałuzińska-Kołat Ż, Celik I, Kontek R. Doxorubicin—An Agent with Multiple Mechanisms of Anticancer Activity. Cells. 2023; 12(4).
57. Tacar O, Sriamornsak P, Dass CR. Doxorubicin: an update on anticancer molecular action, toxicity and novel drug delivery systems. Journal of Pharmacy and Pharmacology. 2013;65(2):157-170.
58. Uceda-Castro R, Margarido AS, Cornet L, Vegna S, Hahn K, Song JY, Putavet DA, van Geldorp M, Çitirikkaya CH, de Keizer PLJ, Ter Beek LC, Borst GR, Akkari L, van Tellingen O, Broekman MLD, Vennin C, van Rheenen J. Re-purposing the pro-senescence properties of doxorubicin to introduce immunotherapy in breast cancer brain metastasis. Cell reports Medicine. 2022;3(11):100821.

59. Chatterjee K, Zhang J, Honbo N, Karliner JS. Doxorubicin cardiomyopathy. Cardiology. 2010;115(2):155-162.
60. Bhinge KN, Gupta V, Hosain SB, Satyanarayanajois SD, Meyer SA, Blaylock B, Zhang QJ, Liu YY. The opposite effects of doxorubicin on bone marrow stem cells versus breast cancer stem cells depend on glucosylceramide synthase. The international journal of biochemistry & cell biology. 2012;44(11):1770-1808.
61. Rahman AM, Yusuf SW, Ewer MS. Anthracycline-induced cardiotoxicity and the cardiac-sparing effect of liposomal formulation. International journal of nanomedicine. 2007;2(4):567-583.
62. Hequet O, Le QH, Moullet I, Pauli E, Salles G, Espinouse D, Dumontet C, Thieblemont C, Arnaud P, Antal D, Bouafia F, Coiffier B. Subclinical late cardiomyopathy after doxorubicin therapy for lymphoma in adults. Journal of clinical oncology : official journal of the American Society of Clinical Oncology. 2004;22(10):1864-1871.
63. Danúbia Silva dos S, Regina Coeli dos Santos G. Doxorubicin-Induced Cardiotoxicity: From Mechanisms to Development of Efficient Therapy. In: Wenyong T, editor. Cardiotoxicity. Rijeka: IntechOpen; 2018. p. Ch. 1.
64. Kinoshita T, Yuzawa H, Natori K, Wada R, Yao S, Yano K, Akitsu K, Koike H, Shinohara M, Fujino T, Shimada H, Ikeda T. Early electrocardiographic indices for predicting chronic doxorubicin-induced cardiotoxicity. Journal of cardiology. 2021;77(4):388-394.
65. Wenningmann N, Knapp M, Ande A, Vaidya TR, Ait-Oudhia S. Insights into Doxorubicin-induced Cardiotoxicity: Molecular Mechanisms, Preventive Strategies, and Early Monitoring. Molecular pharmacology. 2019;96(2):219-232.
66. Mitry MA, Edwards JG. Doxorubicin induced heart failure: Phenotype and molecular mechanisms. International journal of cardiology Heart & vasculature. 2016;10:17-24.
67. Aloss K, Hamar P. Recent Preclinical and Clinical Progress in Liposomal Doxorubicin. Pharmaceutics. 2023; 15(3).
68. O'Brien MER, Wigler N, Inbar M, Rosso R, Grischke E, Santoro A, Catane R, Kieback DG, Tomczak P, Ackland SP, Orlandi F, Mellars L, Alland L, Tendler C. Reduced cardiotoxicity and comparable efficacy in a phase IIItrial of pegylated liposomal

doxorubicin HCl(CAELYX™/Doxil®) versus conventional doxorubicin forfirst-line treatment of metastatic breast cancer. Annals of Oncology. 2004;15(3):440-509.
69. Batist G, Ramakrishnan G, Rao CS, Chandrasekharan A, Gutheil J, Guthrie T, Shah P, Khojasteh A, Nair MK, Hoelzer K, Tkaczuk K, Park YC, Lee LW. Reduced cardiotoxicity and preserved antitumor efficacy of liposome-encapsulated doxorubicin and cyclophosphamide compared with conventional doxorubicin and cyclophosphamide in a randomized, multicenter trial of metastatic breast cancer. Journal of clinical oncology : official journal of the American Society of Clinical Oncology. 2001;19(5):1444-1454.
70. Li S-D, Huang L. Pharmacokinetics and Biodistribution of Nanoparticles. Molecular Pharmaceutics. 2008;5(4):496-504.
71. Gabizon A, Shmeeda H, Barenholz Y. Pharmacokinetics of pegylated liposomal Doxorubicin: review of animal and human studies. Clinical pharmacokinetics. 2003;42(5):419-436.
72. Gabizon A, Shmeeda H, Barenholz Y. Pharmacokinetics of Pegylated Liposomal Doxorubicin. Clinical Pharmacokinetics. 2003;42(5):419-436.
73. Lorusso D, Di Stefano A, Carone V, Fagotti A, Pisconti S, Scambia G. Pegylated liposomal doxorubicin-related palmar-plantar erythrodysesthesia (‘hand-foot’ syndrome). Annals of Oncology. 2007;18(7):1159-1164.
74. Lyass O, Uziely B, Ben-Yosef R, Tzemach D, Heshing NI, Lotem M, Brufman G, Gabizon A. Correlation of toxicity with pharmacokinetics of pegylated liposomal doxorubicin (Doxil) in metastatic breast carcinoma. Cancer. 2000;89(5):1037-1047.
75. Brucker J, Mayer C, Gebauer G, Mallmann P, Belau AK, Schneeweiss A, Sohn C, Eichbaum M. Non-pegylated liposomal doxorubicin for patients with recurrent ovarian cancer: A multicentric phase II trial. Oncology letters. 2016;12(2):1211-1305.
76. Zhao Y, Alakhova DY, Kim JO, Bronich TK, Kabanov AV. A simple way to enhance Doxil® therapy: drug release from liposomes at the tumor site by amphiphilic block copolymer. Journal of controlled release : official journal of the Controlled Release Society. 2013;168(1):61-109.
77. Seynhaeve ALB, Dicheva BM, Hoving S, Koning GA, Ten Hagen TLM. Intact Doxil is taken up intracellularly and released doxorubicin sequesters in the lysosome: evaluated by in vitro/in vivo live cell imaging. Journal of controlled release : official journal of the Controlled Release Society. 2013;172(1):330-340.

78. Prabhakar U, Maeda H, Jain RK, Sevick-Muraca EM, Zamboni W, Farokhzad OC, Barry ST, Gabizon A, Grodzinski P, Blakey DC. Challenges and key considerations of the enhanced permeability and retention effect for nanomedicine drug delivery in oncology. Cancer Res. 2013;73(8):2412-2507.
79. Tanaka HY, Kano MR. Stromal barriers to nanomedicine penetration in the pancreatic tumor microenvironment. Cancer science. 2018;109(7):2085-2092.
80. Vinhas R, Mendes R, Fernandes AR, Baptista PV. Nanoparticles-Emerging Potential for Managing Leukemia and Lymphoma. Frontiers in bioengineering and biotechnology. 2017;5:79.
81. Heldin C-H, Rubin K, Pietras K, Östman A. High interstitial fluid pressure — an obstacle in cancer therapy. Nature Reviews Cancer. 2004;4(10):806-813.
82. Ali ES, Sharker SM, Islam MT, Khan IN, Shaw S, Rahman MA, Uddin SJ, Shill MC, Rehman S, Das N, Ahmad S, Shilpi JA, Tripathi S, Mishra SK, Mubarak MS. Targeting cancer cells with nanotherapeutics and nanodiagnostics: Current status and future perspectives. Seminars in cancer biology. 2021;69:52-68.
83. Li Z, Yin P. Tumor microenvironment diversity and plasticity in cancer multidrug resistance. Biochimica et Biophysica Acta (BBA) - Reviews on Cancer. 2023;1878(6):188997.
84. Aloss K, Hamar P. Augmentation of the EPR effect by mild hyperthermia to improve nanoparticle delivery to the tumor. Biochimica et Biophysica Acta (BBA) - Reviews on Cancer. 2024;1879(4):189109.
85. Kneidl B, Peller M, Winter G, Lindner LH, Hossann M. Thermosensitive liposomal drug delivery systems: state of the art review. International journal of nanomedicine. 2014;9:4387-4398.
86. Leekumjorn S, Sum AK. Molecular studies of the gel to liquid-crystalline phase transition for fully hydrated DPPC and DPPE bilayers. Biochimica et Biophysica Acta (BBA) - Biomembranes. 2007;1768(2):354-365.
87. Li J, Wang X, Zhang T, Wang C, Huang Z, Luo X, Deng Y. A review on phospholipids and their main applications in drug delivery systems. Asian Journal of Pharmaceutical Sciences. 2015;10(2):81-98.

88. Yatvin MB, Weinstein JN, Dennis WH, Blumenthal R. Design of Liposomes for Enhanced Local Release of Drugs by Hyperthermia. Science (New York, NY). 1978;202(4374):1290-1303.
89. Arouri A, Mouritsen OG. Membrane-perturbing effect of fatty acids and lysolipids. Progress in Lipid Research. 2013;52(1):130-140.
90. Landon CD, Park JY, Needham D, Dewhirst MW. Nanoscale Drug Delivery and Hyperthermia: The Materials Design and Preclinical and Clinical Testing of Low Temperature-Sensitive Liposomes Used in Combination with Mild Hyperthermia in the Treatment of Local Cancer. The open nanomedicine journal. 2011;3:38-64.
91. Mills JK, Needham D. Lysolipid incorporation in dipalmitoylphosphatidylcholine bilayer membranes enhances the ion permeability and drug release rates at the membrane phase transition. Biochimica et Biophysica Acta (BBA) - Biomembranes. 2005;1716(2):77-96.
92. de Matos MBC, Beztsinna N, Heyder C, Fens MHAM, Mastrobattista E, Schiffelers RM, Leneweit G, Kok RJ. Thermosensitive liposomes for triggered release of cytotoxic proteins. European Journal of Pharmaceutics and Biopharmaceutics. 2018;132:211-221.
93. Aloss K, Bokhari SM, Leroy Viana PH, Giunashvili N, Schvarcz CA, Szénási G, Bócsi D, Koós Z, Storm G, Miklós Z, Benyó Z, Hamar P. Modulated Electro-Hyperthermia Accelerates Tumor Delivery and Improves Anticancer Activity of Doxorubicin Encapsulated in Lyso-Thermosensitive Liposomes in 4T1-Tumor-Bearing Mice. International Journal of Molecular Sciences. 2024; 25(6).
94. Needham D, Anyarambhatla G, Kong G, Dewhirst MW. A new temperature-sensitive liposome for use with mild hyperthermia: characterization and testing in a human tumor xenograft model. Cancer Res. 2000;60(5):1197-2201.
95. Kong G, Anyarambhatla G, Petros WP, Braun RD, Colvin OM, Needham D, Dewhirst MW. Efficacy of liposomes and hyperthermia in a human tumor xenograft model: importance of triggered drug release. Cancer Res. 2000;60(24):6950-7007.
96. Manzoor AA, Lindner LH, Landon CD, Park JY, Simnick AJ, Dreher MR, Das S, Hanna G, Park W, Chilkoti A, Koning GA, ten Hagen TL, Needham D, Dewhirst MW. Overcoming limitations in nanoparticle drug delivery: triggered, intravascular release to improve drug penetration into tumors. Cancer Res. 2012;72(21):5566-5575.

97. Al-Jamal WT, Kostarelos K. Mild hyperthermia accelerates doxorubicin clearance from tumour-extravasated temperature-sensitive liposomes. Nanotheranostics. 2022;6(3):230-242.
98. Besse HC, Barten-van Rijbroek AD, van der Wurff-Jacobs KMG, Bos C, Moonen CTW, Deckers R. Tumor Drug Distribution after Local Drug Delivery by Hyperthermia, In Vivo. Cancers. 2019; 11(10).
99. Ponce AM, Viglianti BL, Yu D, Yarmolenko PS, Michelich CR, Woo J, Bally MB, Dewhirst MW. Magnetic Resonance Imaging of Temperature-Sensitive Liposome Release: Drug Dose Painting and Antitumor Effects. JNCI: Journal of the National Cancer Institute. 2007;99(1):53-63.
100. Hauck ML, LaRue SM, Petros WP, Poulson JM, Yu D, Spasojevic I, Pruitt AF, Klein A, Case B, Thrall DE, Needham D, Dewhirst MW. Phase I trial of doxorubicin-containing low temperature sensitive liposomes in spontaneous canine tumors. Clinical cancer research : an official journal of the American Association for Cancer Research. 2006;12(13):4004-4010.
101. Mikhail AS, Negussie AH, Pritchard WF, Haemmerich D, Woods D, Bakhutashvili I, Esparza-Trujillo J, Brancato SJ, Karanian J, Agarwal PK, Wood BJ. Lyso-thermosensitive liposomal doxorubicin for treatment of bladder cancer. International Journal of Hyperthermia. 2017;33(7):733-740.
102. Poon RTP, Borys N. Lyso-thermosensitive liposomal doxorubicin: a novel approach to enhance efficacy of thermal ablation of liver cancer. Expert Opinion on Pharmacotherapy. 2009;10(2):333-343.
103. Tak WY, Lin SM, Wang Y, Zheng J, Vecchione A, Park SY, Chen MH, Wong S, Xu R, Peng CY, Chiou YY, Huang GT, Cai J, Abdullah BJJ, Lee JS, Lee JY, Choi JY, Gopez-Cervantes J, Sherman M, Finn RS, Omata M, O'Neal M, Makris L, Borys N, Poon R, Lencioni R. Phase III HEAT Study Adding Lyso-Thermosensitive Liposomal Doxorubicin to Radiofrequency Ablation in Patients with Unresectable Hepatocellular Carcinoma Lesions. Clinical cancer research : an official journal of the American Association for Cancer Research. 2018;24(1):73-83.
104. Lencioni R, Cioni D. RFA plus lyso-thermosensitive liposomal doxorubicin: in search of the optimal approach to cure intermediate-size hepatocellular carcinoma. Hepatic oncology. 2016;3(3):193-200.

105. Dou Y, Hynynen K, Allen C. To heat or not to heat: Challenges with clinical translation of thermosensitive liposomes. Journal of Controlled Release. 2017;249:63-73.
106. Regenold M, Bannigan P, Evans JC, Waspe A, Temple MJ, Allen C. Turning down the heat: The case for mild hyperthermia and thermosensitive liposomes. Nanomedicine: Nanotechnology, Biology and Medicine. 2022;40:102484.
107. Patocka J, Nepovimova E, Wu W, Kuca K. Digoxin: Pharmacology and toxicology-A review. Environmental toxicology and pharmacology. 2020;79:103400.
108. Trenti A, Zulato E, Pasqualini L, Indraccolo S, Bolego C, Trevisi L. Therapeutic concentrations of digitoxin inhibit endothelial focal adhesion kinase and angiogenesis induced by different growth factors. British journal of pharmacology. 2017;174(18):3094-3106.
109. Wang Y, Hou Y, Hou L, Wang W, Li K, Zhang Z, Du B, Kong D. Digoxin exerts anticancer activity on human nonsmall cell lung cancer cells by blocking PI3K/Akt pathway. Bioscience reports. 2021;41(10).
110. Zhao YT, Yan JY, Han XC, Niu FL, Zhang JH, Hu WN. Anti-proliferative effect of digoxin on breast cancer cells via inducing apoptosis. European review for medical and pharmacological sciences. 2017;21(24):5837-5842.
111. Wang Y, Ma Q, Zhang S, Liu H, Zhao B, Du B, Wang W, Lin P, Zhang Z, Zhong Y, Kong D. Digoxin Enhances the Anticancer Effect on Non-Small Cell Lung Cancer While Reducing the Cardiotoxicity of Adriamycin. Frontiers in pharmacology. 2020;11:186.
112. Svensson A, Azarbayjani F, Bäckman U, Matsumoto T, Christofferson R. Digoxin inhibits neuroblastoma tumor growth in mice. Anticancer research. 2005;25(1a):207-212.
113. Zhou Y, Zhou Y, Yang M, Wang K, Liu Y, Zhang M, Yang Y, Jin C, Wang R, Hu R. Digoxin sensitizes gemcitabine-resistant pancreatic cancer cells to gemcitabine via inhibiting Nrf2 signaling pathway. Redox Biology. 2019;22:101131.
114. Gayed BA, O'Malley KJ, Pilch J, Wang Z. Digoxin inhibits blood vessel density and HIF-1a expression in castration-resistant C4-2 xenograft prostate tumors. Clinical and translational science. 2012;5(1):39-42.
115. Zhang Z, Wang Y, Ma Q, Zhang S, Liu H, Zhao B, Liu R, Wang W, Du B, Zhong Y, Kong D. Biomimetic carrier-free nanoparticle delivers digoxin and doxorubicin to

exhibit synergetic antitumor activity in vitro and in vivo. Chemical Engineering Journal. 2021;406:126801.
116. Lyon PC, Griffiths LF, Lee J, Chung D, Carlisle R, Wu F, Middleton MR, Gleeson FV, Coussios CC. Clinical trial protocol for TARDOX: a phase I study to investigate the feasibility of targeted release of lyso-thermosensitive liposomal doxorubicin (ThermoDox®) using focused ultrasound in patients with liver tumours. Journal of therapeutic ultrasound. 2017;5:28.
117. Zagar TM, Vujaskovic Z, Formenti S, Rugo H, Muggia F, O'Connor B, Myerson R, Stauffer P, Hsu IC, Diederich C, Straube W, Boss MK, Boico A, Craciunescu O, Maccarini P, Needham D, Borys N, Blackwell KL, Dewhirst MW. Two phase I dose-escalation/pharmacokinetics studies of low temperature liposomal doxorubicin (LTLD) and mild local hyperthermia in heavily pretreated patients with local regionally recurrent breast cancer. International journal of hyperthermia : the official journal of European Society for Hyperthermic Oncology, North American Hyperthermia Group. 2014;30(5):285-294.
118. de Maar JS, Suelmann BBM, Braat M, van Diest PJ, Vaessen HHB, Witkamp AJ, Linn SC, Moonen CTW, van der Wall E, Deckers R. Phase I feasibility study of Magnetic Resonance guided High Intensity Focused Ultrasound-induced hyperthermia, Lyso-Thermosensitive Liposomal Doxorubicin and cyclophosphamide in de novo stage IV breast cancer patients: study protocol of the i-GO study. BMJ open. 2020;10(11):e040162.
119. Sun M, Chen M, Wang M, Hansen J, Baatrup A, Dagnaes-Hansen F, Rölfing JHD, Jensen J, Lysdahl H, Li H, Johannsen M, Le DQS, Kjems J, Bünger CE. In vivo drug release behavior and osseointegration of a doxorubicin-loaded tissue-engineered scaffold. RSC Advances. 2016;6(80):76237-76245.
120. Vancsik T, Kovago C, Kiss E, Papp E, Forika G, Benyo Z, Meggyeshazi N, Krenacs T. Modulated electro-hyperthermia induced loco-regional and systemic tumor destruction in colorectal cancer allografts. Journal of Cancer. 2018;9(1):41-53.
121. Bokhari SMZ, Aloss K, Leroy Viana PH, Schvarcz CA, Besztercei B, Giunashvili N, Bócsi D, Koós Z, Balogh A, Benyó Z, Hamar P. Digoxin-Mediated Inhibition of Potential Hypoxia-Related Angiogenic Repair in Modulated Electro-Hyperthermia

(mEHT)-Treated Murine Triple-Negative Breast Cancer Model. ACS Pharmacology & Translational Science. 2024;7(2):456-466.
122. Needham D, Anyarambhatla G, Kong G, Dewhirst MW. A New Temperature-sensitive Liposome for Use with Mild Hyperthermia: Characterization and Testing in a Human Tumor Xenograft Model1. Cancer Research. 2000;60(5):1197-1201.
123. Mikhail AS, Negussie AH, Pritchard WF, Haemmerich D, Woods D, Bakhutashvili I, Esparza-Trujillo J, Brancato SJ, Karanian J, Agarwal PK, Wood BJ. Lyso-thermosensitive liposomal doxorubicin for treatment of bladder cancer. International journal of hyperthermia : the official journal of European Society for Hyperthermic Oncology, North American Hyperthermia Group. 2017;33(7):733-740.
124. Wust P, Kortüm B, Strauss U, Nadobny J, Zschaeck S, Beck M, Stein U, Ghadjar P. Non-thermal effects of radiofrequency electromagnetic fields. Scientific reports. 2020;10(1):13488.
125. Yang KL, Huang CC, Chi MS, Chiang HC, Wang YS, Hsia CC, Andocs G, Wang HE, Chi KH. In vitro comparison of conventional hyperthermia and modulated electro-hyperthermia. Oncotarget. 2016;7(51):84082-84092.
126. You SH, Kim S. Feasibility of modulated electro-hyperthermia in preoperative treatment for locally advanced rectal cancer: Early phase 2 clinical results. Neoplasma. 2020;67(3):677-683.
127. Prieto C, Linares I. Nanoparticles and nanothermia for malignant brain tumors, a suggestion of treatment for further investigations. Reports of practical oncology and radiotherapy : journal of Greatpoland Cancer Center in Poznan and Polish Society of Radiation Oncology. 2018;23(5):474-480.
128. Dromi S, Frenkel V, Luk A, Traughber B, Angstadt M, Bur M, Poff J, Xie J, Libutti SK, Li KC, Wood BJ. Pulsed-high intensity focused ultrasound and low temperature-sensitive liposomes for enhanced targeted drug delivery and antitumor effect. Clinical cancer research : an official journal of the American Association for Cancer Research. 2007;13(9):2722-2727.
129. Frenkel V, Oberoi J, Stone MJ, Park M, Deng C, Wood BJ, Neeman Z, Horne M, 3rd, Li KC. Pulsed high-intensity focused ultrasound enhances thrombolysis in an in vitro model. Radiology. 2006;239(1):86-93.

130. Wang S, Frenkel V, Zderic V. Optimization of pulsed focused ultrasound exposures for hyperthermia applications. The Journal of the Acoustical Society of America. 2011;130(1):599-609.
131. Dou Y, Hynynen K, Allen C. To heat or not to heat: Challenges with clinical translation of thermosensitive liposomes. Journal of controlled release : official journal of the Controlled Release Society. 2017;249:63-73.
132. Al-Jamal WT, Al-Ahmady ZS, Kostarelos K. Pharmacokinetics & tissue distribution of temperature-sensitive liposomal doxorubicin in tumor-bearing mice triggered with mild hyperthermia. Biomaterials. 2012;33(18):4608-4617.
133. Al-Ahmady ZS, Scudamore CL, Kostarelos K. Triggered doxorubicin release in solid tumors from thermosensitive liposome-peptide hybrids: Critical parameters and therapeutic efficacy. International journal of cancer. 2015;137(3):731-743.
134. Frenkel V, Etherington A, Greene M, Quijano J, Xie J, Hunter F, Dromi S, Li KC. Delivery of liposomal doxorubicin (Doxil) in a breast cancer tumor model: investigation of potential enhancement by pulsed-high intensity focused ultrasound exposure. Academic radiology. 2006;13(4):469-479.
135. Tsang YW, Chi KH, Huang CC, Chi MS, Chiang HC, Yang KL, Li WT, Wang YS. Modulated electro-hyperthermia-enhanced liposomal drug uptake by cancer cells. International journal of nanomedicine. 2019;14:1269-1279.
136. Maswadeh HM, Khan A, Alorainy MS, Al-Wabel NA, Demetzos C. Concomitant delivery of doxorubicin and cisplatin through liposome-based thermosensitive nanoparticles: perspective in the treatment of cancer in animal models. American journal of cancer research. 2023;13(2):379-793.
137. El-Hamid ESA, Gamal-Eldeen AM, Sharaf Eldeen AM. Liposome-coated nano doxorubicin induces apoptosis on oral squamous cell carcinoma CAL-27 cells. Archives of Oral Biology. 2019;103:47-54.
138. Harmon BV, Corder AM, Collins RJ, Gobé GC, Allen J, Allan DJ, Kerr JF. Cell death induced in a murine mastocytoma by 42-47 degrees C heating in vitro: evidence that the form of death changes from apoptosis to necrosis above a critical heat load. Int J Radiat Biol. 1990;58(5):845-858.
139. Kim M, Kim G, Kim D, Yoo J, Kim DK, Kim H. Numerical Study on Effective Conditions for the Induction of Apoptotic Temperatures for Various Tumor Aspect Ratios

Using a Single Continuous-Wave Laser in Photothermal Therapy Using Gold Nanorods. Cancers (Basel). 2019;11(6).
140. Denard B, Lee C, Ye J. Doxorubicin blocks proliferation of cancer cells through proteolytic activation of CREB3L1. eLife. 2012;1:e00090.
141. Wu SK, Chiang CF, Hsu YH, Lin TH, Liou HC, Fu WM, Lin WL. Short-time focused ultrasound hyperthermia enhances liposomal doxorubicin delivery and antitumor efficacy for brain metastasis of breast cancer. International journal of nanomedicine. 2014;9:4485-4494.
142. Sadeghi N, Deckers R, Ozbakir B, Akthar S, Kok RJ, Lammers T, Storm G. Influence of cholesterol inclusion on the doxorubicin release characteristics of lysolipid-based thermosensitive liposomes. International journal of pharmaceutics. 2018;548(2):778-782.
143. Banno B, Ickenstein LM, Chiu GN, Bally MB, Thewalt J, Brief E, Wasan EK. The functional roles of poly(ethylene glycol)-lipid and lysolipid in the drug retention and release from lysolipid-containing thermosensitive liposomes in vitro and in vivo. Journal of pharmaceutical sciences. 2010;99(5):2295-2308.
144. Besse HC, Barten-van Rijbroek AD, van der Wurff-Jacobs KMG, Bos C, Moonen CTW, Deckers R. Tumor Drug Distribution after Local Drug Delivery by Hyperthermia, In Vivo. Cancers. 2019;11(10).
145. Swenson CE, Haemmerich D, Maul DH, Knox B, Ehrhart N, Reed RA. Increased Duration of Heating Boosts Local Drug Deposition during Radiofrequency Ablation in Combination with Thermally Sensitive Liposomes (ThermoDox) in a Porcine Model. PloS one. 2015;10(10):e0139752.
146. Yarmolenko PS, Zhao Y, Landon C, Spasojevic I, Yuan F, Needham D, Viglianti BL, Dewhirst MW. Comparative effects of thermosensitive doxorubicin-containing liposomes and hyperthermia in human and murine tumours. International journal of hyperthermia : the official journal of European Society for Hyperthermic Oncology, North American Hyperthermia Group. 2010;26(5):485-498.
147. Aloss K, Leroy Viana PH, Bokhari SMZ, Giunashvili N, Schvarcz CA, Bócsi D, Koós Z, Benyó Z, Hamar P. Ivermectin Synergizes with Modulated Electro-hyperthermia and Improves Its Anticancer Effects in a Triple-Negative Breast Cancer Mouse Model. ACS Pharmacol Transl Sci. 2024 Jul 17;7(8):2496-2506

148. Nakamura H, Fang J, Maeda H. Development of next-generation macromolecular drugs based on the EPR effect: challenges and pitfalls. Expert opinion on drug delivery. 2015;12(1):53-64.
149. Lin J, Zhan T, Duffy D, Hoffman-Censits J, Kilpatrick D, Trabulsi EJ, Lallas CD, Chervoneva I, Limentani K, Kennedy B, Kessler S, Gomella L, Antonarakis ES, Carducci MA, Force T, Kelly WK. A pilot phase II Study of digoxin in patients with recurrent prostate cancer as evident by a rising PSA. American journal of cancer therapy and pharmacology. 2014;2(1):21-32.

9. Bibliography of the candidate's publications

Publications related to the thesis

Aloss, K.; Bokhari, S.M.Z.; Leroy Viana, P.H.; Giunashvili, N.; Schvarcz, C.A.; Szénási, G.; Bócsi, D.; Koós, Z.; Storm, G.; Miklós, Z.; et al. Modulated Electro-Hyperthermia Accelerates Tumor Delivery and Improves Anticancer Activity of Doxorubicin Encapsulated in Lyso-Thermosensitive Liposomes in 4T1-Tumor-Bearing Mice. Int. J. Mol. Sci. 2024, 25, 3101. https://doi.org/10.3390/ijms25063101. Impact factor: 5.6

Bokhari SMZ, **Aloss K**, Leroy Viana PH, Schvarcz CA, Besztercei B, Giunashvili N, Bócsi D, Koós Z, Balogh A, Benyó Z, Hamar P. Digoxin-Mediated Inhibition of Potential Hypoxia-Related Angiogenic Repair in Modulated Electro-Hyperthermia (mEHT)-Treated Murine Triple-Negative Breast Cancer Model. ACS Pharmacol Transl Sci. 2024 Jan 9;7(2):456-466. doi: 10.1021/acsptsci.3c00296. Impact factor: 6

Aloss K, Hamar P. Recent Preclinical and Clinical Progress in Liposomal Doxorubicin. Pharmaceutics. 2023 Mar 9;15(3):893. doi: 10.3390/pharmaceutics15030893. Impact factor: 5.4

Aloss K, Hamar P. Augmentation of the EPR effect by mild hyperthermia to improve nanoparticle delivery to the tumor. Biochimica et Biophysica Acta (BBA) - Reviews on Cancer, 2024. 1879(4): p. 189109. Impact factor: 11.2

Publications not related to the thesis

Aloss K, Leroy Viana PH, Bokhari SMZ, Giunashvili N, Schvarcz CA, Bócsi D, Koós Z, Benyó Z, Hamar P. Ivermectin Synergizes with Modulated Electro-hyperthermia and Improves Its Anticancer Effects in a Triple-Negative Breast Cancer Mouse Model. ACS Pharmacol Transl Sci. 2024 Jul 17;7(8):2496-2506. Impact factor: 4.9

Giunashvili N, Thomas JM, Schvarcz CA, Viana PHL, **Aloss K**, Bokhari SMZ, Koós Z, Bócsi D, Major E, Balogh A, Benyó Z, Hamar P. Enhancing therapeutic efficacy in triple-negative breast cancer and melanoma: synergistic effects of modulated electro-hyperthermia (mEHT) with NSAIDs especially COX-2 inhibition in *in vivo* models. Mol Oncol. 2024 Jan 12. doi: 10.1002/1878-0261.13585. Impact factor: 6.6

Pedro H L Viana, Csaba A Schvarcz, Lea O Danics, Balázs Besztercei, **Kenan Aloss**, Syeda M Z Bokhari, Nino Giunashvili, Dániel Bócsi, Zoltán Koós, Zoltán Benyó, Péter Hamar. Heat shock factor 1 inhibition enhances the effects of modulated electro hyperthermia in a triple negative breast cancer mouse model. Sci Rep 14, 8241 (2024). Impact factor: 4.6

Dora, D.; Bokhari, S.M.Z.; **Aloss, K**.; Takacs, P.; Desnoix, J.Z.; Szklenárik, G.; Hurley, P.D.; Lohinai, Z. Implication of the Gut Microbiome and Microbial-Derived Metabolites in Immune-Related Adverse Events: Emergence of Novel Biomarkers for Cancer Immunotherapy. Int. J. Mol. Sci. 2023, 24, 2769. Impact factor: 5.6

10. Acknowledgments

I would like to express my deepest gratitude to my supervisor, Professor Péter Hamar, for his guidance, encouragement, and support throughout the course of this research. His expertise and insights have been instrumental in shaping this thesis.

I am grateful to my internal defense reviewer, Gábor Szénási, for his valuable comments and suggestions which helped to improve my thesis.

I am also profoundly thankful to the head of the doctoral school, Professor Zoltan Benyó for his big support during my PhD study

My heartfelt thanks go to my colleagues, Nino Giunashvili, Pedro Viana, Syeda Bokhari, and Csaba Schvarcz, whose collaborative spirit has made this journey both enjoyable and enriching. I am also grateful to Zoltán Koós and Dániel Bócsi for their administrative help.

Lastly, I owe my deepest appreciation to my family, whose unwavering support and understanding have been my anchor throughout this academic endeavor.

This thesis would not have been possible without the encouragement of those mentioned above.